Vangl2 suppresses NF-κB signaling and ameliorates sepsis by targeting p65 for NDP52-mediated autophagic degradation

Jiansen Lu[1,2,10], Jiahuan Zhang[3,4,10], Huaji Jiang[1,5,10], Zhiqiang Hu[1,10], Lian He[6,7], Jianwu Yang[1], Yingchao Xie[1], Dan Wu[1], Hongyu Li[1], Ke Zeng[1], Peng Tan[8], Qingyue Xiao[3], Zijing Song[3], Xiaochun Bai[3*] and Xiao Yu[1,9*]

[1]Department of Immunology, School of Basic Medical Sciences, Southern Medical University, Guangzhou, Guangdong 510515, China

[2]Department of Joint Surgery, the Fifth Affiliated Hospital, Southern Medical University, Guangzhou, Guangdong 510515, China

[3]Department of Cell Biology, School of Basic Medical Sciences, Southern Medical University, Guangzhou, Guangdong 510515, China

[4]Laboratory Medicine, Guangdong Provincial People's Hospital (Guangdong Academy of Medical Sciences), Southern Medical University, Guangzhou, Guangdong 510515, China

[5]Department of Orthopaedics, Yue Bei People's Hospital Affiliated to Medical College of Shantou University, Shaoguan 512026, China

[6]Department of Pharmacology, School of Medicine, Southern University of Science and Technology, Shenzhen, Guangdong 518005, China

[7]Institute of Biosciences and Technology, College of Medicine, Texas A&M University, Houston, Texas 77030, USA

[8]Klarman Cell Observatory, Broad Institute of MIT and Harvard, Cambridge, Massachusetts 02142, USA

[9]Guangdong Provincial Key Lab of Single Cell Technology and Application, Southern Medical University, Guangzhou, Guangdong 510515, China

[10]These authors contribute equally.

*Correspondence: X.Y. (xiaoyu523@smu.edu.cn), X.B. (baixc15@smu.edu.cn)

Abstract

Van Gogh-like 2 (Vangl2), a core planar cell polarity (PCP) component, plays an important role in polarized cellular and tissue morphology induction, growth development and cancer. However, its role in regulating inflammatory responses remains elusive. Here, we report that Vangl2 is upregulated in patients with sepsis and identify Vangl2 as a negative regulator of NF-κB signaling by regulating the protein stability and activation of the core transcription component p65. Mice with myeloid-specific deletion of Vangl2 (*Vangl2*$^{\Delta M}$) are hypersusceptible to lipopolysaccharide (LPS)-induced septic shock. Vangl2 deficient myeloid cells exhibit enhanced phosphorylation and expression of p65, therefore, promoting the secretion of pro-inflammatory cytokines after LPS stimulation. Mechanistically, NF-κB signaling-induced-Vangl2 recruits E3 ubiquitin ligase PDLIM2 to catalyze K63-linked ubiquitination on p65, which serves as a recognition signal for cargo receptor NDP52-mediated selective autophagic degradation. Taken together, these findings demonstrate Vangl2 as a suppressor of NF-κB mediated inflammation and provide insights into the crosstalk between autophagy and inflammatory diseases.

63 **Introduction**

64 Vangl2, a core PCP component, mediates Wingless-type (Wnt)/PCP signaling, and
65 controls homeostasis, development, and repair of organs (Bailly, Walton, & Borg, 2018;
66 Brunt et al., 2021; Hatakeyama, Wald, Printsev, Ho, & Carraway, 2014). Vangl2 has four
67 transmembrane domains with both carboxyl termini and amino oriented toward the
68 cytoplasm, which is phosphorylated in the endoplasmic reticulum (ER) and then
69 transported to the cell surface and becomes stabilized, while the unphosphorylated
70 Vangl2 is unstable and internalized to degrade via the lysosomal pathway (D. Feng et al.,
71 2021). The shuttle of Vangl2 between cytoplasm and cell membrane results in its
72 multifunction, including adhesion, membrane protrusive activity, migration, and bridging
73 proteins (Hatakeyama et al., 2014). Indeed, Vangl2 inhibited matrix metalloproteinase 2
74 (MMP2) activity and affected cell adhesion to extracellular matrix proteins (Jessen &
75 Jessen, 2017). Vangl2 also modulates glomerular injury by promoting MMP9
76 (Papakrivopoulou et al., 2018). Moreover, the abnormal function of Vangl2 results in
77 various diseases, such as cancer, kidney glomerular injury, idiopathic pulmonary fibrosis
78 and systemic dysplasia (Papakrivopoulou et al., 2018; Poobalasingam et al., 2017).
79 Vangl2 is markedly down-regulated in patients with emphysema (Poobalasingam et al.,
80 2017), while which level was up-regulated and amplified in breast, ovarian, and uterine
81 carcinomas (Cancer Genome Atlas Research et al., 2013; Cerami et al., 2012; Gao et
82 al., 2013). In addition, Vangl2 is bounded to p62 to promote breast cancer
83 (Puvirajesinghe et al., 2016). Our previous study showed that Vangl2 prevents
84 osteogenic differentiation in mesenchymal stem cells, resulting in osteogenic dysplasia
85 (Gong et al., 2021). Vangl2 mediated downstream of Toll-like or interleukin (IL)-1
86 receptor, such as myeloid differentiation factor 88 (MyD88) (Gong et al., 2021),
87 suggesting that Vangl2 may play roles in immune-related diseases, including
88 autoimmune diseases. However, the function of Vangl2 in inflammatory diseases
89 remains uncovered.

90 The NF-κB signaling is critical for the pathogenesis of a number of inflammatory
91 diseases, such as inflammatory bowel disease (IBD), rheumatoid arthritis (RA), systemic
92 lupus erythematosus (SLE) and sepsis (Liu, Zhang, Joo, & Sun, 2017). NF-κB activation
93 relies on the pattern recognition receptors (PRRs) recognition of pathogen-associated
94 molecular patterns (PAMPs), including Toll like receptor (TLR), NOD-like receptors
95 (NLRs) and RIG-I-like receptors (RLRs) (Liu et al., 2017). LPS triggers TLR activation
96 and the recruitment of adaptor proteins including MyD88. This in turn activates a series

97 of downstream canonical NF-κB signaling cascade, resulting in the phosphorylation and
98 degradation of IκB and the nuclear translocation of RelA/p65 and p50 to induce the
99 transcription of several inflammatory cytokines, such as interleukin (IL)-1, IL-6, and
100 tumor necrosis factor-α (TNF-α) (Funes, Rios, Escobar-Vera, & Kalergis, 2018; Locati,
101 Curtale, & Mantovani, 2020). Since uncontrolled immune responses are detrimental to
102 the host, inappropriate or excessive NF-κB activity contributes to the pathogenesis of
103 various inflammatory diseases and cancer (Cartwright, Perkins, & C, 2016). Thus NF-κB
104 signaling must be tightly regulated to maintain immune balance in the organism. In
105 recent decades, extensive studies have focused on the mechanisms underlying the
106 regulation of NF-κB signaling. Recent research demonstrated that NLRC5 strongly
107 prevents NF-κB signaling pathway by interacting with IκB kinase (IKK) α/IKKβ and
108 blocking their phosphorylation (Cui et al., 2010). COMMD1, PPARγ, SOCS1 and GCN5
109 were also shown to negatively regulate NF-κB signaling (Bartuzi, Hofker, & van de Sluis,
110 2013; Mao et al., 2009). Meanwhile, tripartite motif-containing protein 21 (Trim21)
111 enhanced the interaction of p65 with IKK, which promotes p65 phosphorylation and
112 downstream gene activation (Yang et al., 2021). However, the molecular mechanisms
113 underpinning the regulation of NF-κB signaling are still elusive.

114 Autophagy, a conserved intracellular degradation pathway, decomposes
115 cytoplasmic organelles and components, and acts as a defense mechanism to pathogen
116 infection, playing a crucial role in nutrient recycling, stress response and cellular
117 homeostasis (Ashrafi & Schwarz, 2013; Denton & Kumar, 2019). Recent evidence
118 indicates that autophagy is highly selective when delivering specific substrates to
119 autolysosomal degradation by virtue of a number of cargo receptors, including
120 sequestosome 1 (SQSTM1/p62), optineurin (OPTN), nuclear dot protein 52
121 (NDP52/CALCOCO2) and neighbor of BRCA1 (NBR1) (Gatica, Lahiri, & Klionsky, 2018).
122 Selective autophagy targets immune regulators for degradation, thus suppressing innate
123 immune signaling, such as type I IFN and NF-κB signaling (Pradel, Robert-Hebmann, &
124 Espert, 2020; Tong et al., 2012). Moreover, p62 protein has been identified as a novel
125 Vangl2-binding partner (Puvirajesinghe et al., 2016), and our recent study has
126 demonstrated that Vangl2 reduces lysosomal chaperone-mediated autophagy (CMA)
127 activity by targeting LAMP-2A for degradation (Gong et al., 2021). However, whether
128 and how Vangle2 is involved in the selective autophagic regulation of NF-κB signaling
129 remains largely unknown.

130 In this study, we uncover a previously unrecognized role of Vangl2, as a "molecular
131 brake", in the negative regulation of NF-κB signaling to prevent excessive and potentially
132 harmful immune responses during sepsis in both human patient samples and LPS
133 induced mouse model. Induction of Vangl2 upon inflammation recruits an E3 ubiquitin
134 ligase PDLIM2 to catalyze K63-linked ubiquitination on p65, thus promoting the
135 recognition of p65 by the cargo receptor NDP52 and resulting in the selective autophagic
136 degradation of p65. Our findings provide a potential target for the treatment of
137 inflammatory diseases.
138
139 **Results**
140 **Loss of Vangl2 promotes inflammatory responses in LPS-induced septic shock.**
141 To investigate the potential role of Vangl2 in inflammatory response, we first analyzed
142 the expression of Vangl2 in peripheral blood mononuclear cells (PBMCs) from sepsis
143 patients (Fig. S1 A) and found mRNA level of Vangl2 was increased in the sepsis
144 patients compared to healthy control (HC) (Fig. 1 A). Expression of Vangl2 from
145 database GSE156382 also confirmed that Vangl2 mRNA was induced during sepsis (Fig.
146 S1 B). To further determine whether *Vangl2* expression could be regulated in response
147 to inflammatory stimulation, we treated mice with LPS to activate NF-κB pathway and
148 detected *Vangl2* mRNA in different tissues from LPS treated mice, and found the
149 expression of *Vangl2* significantly increased in secondary lymphoid organs including the
150 spleen and lymph nodes after LPS stimulation, but not in other tissues (Fig. 1 B).
151 Moreover, qPCR and western blot analyses revealed strong upregulation of *Vangl2* at
152 both the mRNA and protein levels after LPS stimulation in bone marrow (BM)-derived
153 macrophages (BMDMs), neutrophils and peritoneal macrophages (Fig. S1, C-E),
154 suggesting that Vangl2 is induced in immune organ tissues and cells in response to
155 inflammation.
156 To determine the function of Vangl2 during LPS-induced sepsis, we specifically
157 ablated Vangl2 in myeloid cells by crossing *Vangl2*$^{flox/flox}$ mice with mice expressing
158 lysozyme proximal promoter (*Lyz2-Cre*). The resultant homozygous *Vangl2*$^{flox/flox}$ × *Lyz2-*
159 *Cre* mice were designated *Vangl2*$^{\Delta M}$ mice and selective deletion of Vangl2 in myeloid
160 cells of *Vangl2*$^{\Delta M}$ mice were confirmed by PCR (Fig. S1 F). Although there were no
161 significant differences in the size of spleen and lymph nodes between wild-type (WT)
162 and *Vangl2*$^{\Delta M}$ mice (Fig. S1 G), myeloid-specific loss of Vangl2 increased the number of
163 monocytes, macrophages and neutrophils in the spleen and bone marrow (Fig. S1, H

164 and I). To gain further insight into the physiological function of Vangl2, we treated WT
165 and *Vangl2*$^{\Delta M}$ mice with a high dose of LPS and monitored mice survival. We found that
166 all *Vangl2*$^{\Delta M}$ mice died after LPS-induced septic shock within 20 hours, compared to only
167 20% of the WT mice, whereas the remaining WT mice survived for more than 50 hours
168 (Fig. 1 C). Consistent with this observation, *Vangl2*$^{\Delta M}$ mice markedly increased the
169 protein level of IL-1β in isolated CD11b^{+} splenocytes (Fig. 1 D), and mRNA levels of *Il1b*,
170 *Tnfa* and *Il6* in the spleen (Fig. 1 E). Meanwhile, *Vangl2*$^{\Delta M}$ mice showed markedly
171 elevated serum amounts of proinflammatory cytokines such as IL-1β, TNF-α and IL-6
172 after LPS treatment, compared with WT mice (Fig. 1 F). Together, these data provide in
173 vivo evidence that myeloid cell-specific deletion of Vangl2 in mice enhances the
174 sensitivity and severity of LPS-induced septic shock and is associated with increased
175 expression of proinflammatory cytokines.
176
177 **Vangl2 negatively regulates NF-κB activation and inflammation in myeloid cells.**
178 To investigate the mechanisms by which Vangl2 prevents sepsis, we performed RNA-
179 seq analysis to identify signal pathways involved in LPS-induced septic shock by
180 comparing LPS-stimulated BMDMs from *Vangl2*$^{\Delta M}$ and WT mice. Differentially
181 expression analysis showed 907 up-regulated genes and 1092 down-regulated genes in
182 response to Vangl2 deficiency in BMDMs after LPS stimulation (Fig. S2 A). Gene
183 ontology (GO) analysis further identified that these genes are involved in cellular
184 immune responses, including "cellular response to lipopolysaccharide" (Fig. S2 B) and
185 KEGG analysis revealed genes involved in TNF signaling pathway and cytokine-cytokine
186 receptor interaction were highly enriched in *Vangl2*$^{\Delta M}$ BMDMs after LPS stimulation,
187 suggesting that Vangl2 may regulate these signaling pathways and related cytokines
188 release (Fig. S2 C).
189 To determine the function of Vangl2 in innate immune signaling in myeloid cells, we
190 isolated BMDMs, neutrophils and peritoneal macrophages (pMAC) from WT and
191 *Vangl2*$^{\Delta M}$ mice, treated them with LPS, and performed immunoblot analysis with specific
192 antibodies. We found that phosphorylations of IKK and p65 were enhanced and
193 remained high level for a sustained period in Vangl2-deficient pMAC, neutrophils and
194 BMDMs, compared with WT cells (Fig. 2, A-D and Fig. S2, D and E). Consistent with this
195 observation, Vangl2-deficient macrophages, and neutrophils showed markedly elevated
196 pro-inflammatory cytokines such as TNF-α, IL-6 (Fig. 2 E and F and Fig. S2 F) and IL-1β
197 (Fig. S2 G), after LPS treatment. Moreover, we detected enhanced p65 nuclear

198 accumulation in LPS-induced Vangl2-deficient neutrophils, compared with WT
199 neutrophils (Fig. 2, G and H).
200 To further confirm the function of Vangl2 in regulating NF-κB signaling, we
201 overexpressed Flag-tagged Vangl2 in A549 cells. We found that Vangl2 overexpression
202 inhibited phosphorylation of IKK and p65 in A549 cells (Fig. 2, I and J). These results
203 suggest that Vangl2 prevents LPS-induced NF-κB activation and proinflammatory
204 cytokine production.
205
206 **Vangl2 inhibits LPS-induced NF-κB activation by interacting with p65.**
207 To clarify the regulatory mechanism of Vangl2, we transfected Chinese hamster ovary
208 (CHO) or 293T cells with NF-κB luciferase reporter vector, with or without the Vangl2
209 plasmid, then treated the cells with LPS, IL-1β, or TNF-α. We found that Vangl2
210 markedly inhibited NF-κB activation induced by LPS, IL-1β, or TNF-α in a dose-
211 dependent manner (Fig. 3, A-C). Next, we sought to determine potential signaling
212 molecules that mediated the NF-κB-luc reporter. NF-κB-luc activity was strongly
213 activated by overexpression of MyD88, IRAK1, TRAF6, IKKα, IKKβ or p65, but all of
214 these activities were inhibited when *Vangl2* was co-transfected at increasing
215 concentrations (Fig. 3 D and Fig. S3, A-F), suggesting that Vangl2 may block NF-κB
216 activation at the very downstream signaling level of p65.
217 To test this prediction, we transfected 293T cells with HA-tagged Vangl2 together
218 with Flag-tagged IKKα, p65, TRAF6, IRAK1 or MyD88. Co-immunoprecipitation (co-IP)
219 assay revealed that Vangl2 interacted strongly with IKKα, p65 and MyD88, and weak
220 with TRAF6 or IRAK1 (Fig. 3 E and Fig. S3 G). In addition, endogenous co-IP
221 immunoblot analyses showed that Vangl2 was strongly associated with p65 upon LPS
222 stimulation in BMDMs, but not with IKKα, IKKβ or MyD88 (Fig. 3 F and Fig. S3 H).
223 Moreover, ZDOCK server predicted that Vangl2 may potentially interact with p65 by a
224 hydrogen bond (Fig. S3 I). We further investigated the co-localization of Vangl2 and p65
225 by confocal microscopy and found a weak-co-localization of Vangl2 with p65 in
226 unstimulated cells and the co-localization between Vangl2 and p65 was notably
227 enhanced upon LPS stimulation (Fig. 3 G and Fig. S3 J). To determine how Vangl2
228 interacts with cytoplasmic p65, we isolated cytoplasm and membrane in LPS treated
229 THP-1 cells. We found that Vangl2 interacted with p65 mainly in the cytoplasm, although

230 most of Vangl2 located on the membrane (Fig. S3 K). Together, these data suggest that
231 Vangl2 may interact with p65 in the cytoplasm to inhibit NF-κB signaling.
232 Vangl2 comprises an N-terminal cytoplasmic tail (NT), a transmembrane (TM)
233 domain, a Prickle-binding domain (PkBD), and a C-terminal cytoplasmic tail (CT)
234 (Nagaoka, Furuse, Ohtsuka, Tsuchida, & Kishi, 2019). To map the essential domains of
235 Vangl2 that mediate its association with p65, we generated several deletion constructs
236 of Vangl2. We found Vangl2 FL (full-length), T2 (ΔNT+TM), T3 (ΔCT), and T4 (ΔNT)
237 interacted with the full-length p65, while Vangl2 T1 (ΔPkBD+CT) abrogated their
238 association (Fig. 3 H and Fig. S3 L), indicating that the PkBD domain is important for the
239 Vangl2-p65 interaction. Additionally, we constructed HA-tagged Vangl2 PkBD plasmid
240 and co-IP assay revealed that Vangl2 FL and PkBD interacted with p65 (Fig. 3 I).
241 Moreover, we observed that deletion of the PkBD domain (T1), but not other domains, of
242 Vangl2 abolished the Vangl2-mediated inhibition of NF-κB-luc activity, and transfection
243 of Vangl2 PkBD domain achieved similar inhibition on p65 induced NF-κB activation as
244 Vangl2 FL did (Fig. 3 J). Collectively, these data suggest that Vangl2 suppresses NF-κB
245 signaling by targeting p65 through Vangl2 PkBD domain interaction.
246
247 **Vangl2 promotes the autophagic degradation of p65.**
248 Next we sought to study the physiological role of Vangl2-p65 interaction in the regulation
249 of NF-κB signaling by transfecting 293T cells with Flag-tagged p65, together with
250 increasing doses of Vangl2, and found that Vangl2 dramatically decreased the protein
251 level of p65 in a dose-dependent manner (Fig. 4 A). To exclude the possibility that the
252 downregulation of p65 protein by Vangl2 was caused by the inhibition of p65
253 transcription, qPCR results suggested that the abundance of *p65* mRNA did not change
254 in cells with increased expression of Vangl2 (Fig. 4 B). Since activated p65 translocates
255 to the nucleus, we next assessed whether Vangl2 regulates the degradation of p65 in
256 the cytoplasm or nucleus, and found that the Vangl2 interacted with p65 mainly in the
257 cytoplasm (Fig. S4 A) and mediated the degradation of p65 in the cytoplasmic fraction
258 (Fig. 4 C), which is consistent with the result that Vangl2 and p65 co-localized in the
259 cytoplasm (Fig. 3 G). To further assess whether Vangl2 regulates the degradation of
260 endogenous p65, we found that Vangl2-deficient BMDMs stabilized the expression of
261 endogenous p65 after LPS treatment (Fig. 4 D). After 12 h LPS stimulation,
262 cycloheximide (CHX)-chase assay result showed that the degradation rate of p65 in

263 *Vangl2*$^{\Delta M}$ BMDMs was slower, compared with WT cells (Fig. S4 B). Together, these data
264 suggest that Vangl2 promotes p65 protein degradation.
265 To investigate whether Vangl2 degrades p65 through an autolysosome or
266 proteasome pathway, 293T cells were transfected with p65, together with or without the
267 Vangl2 plasmids, and treated with different pharmacological inhibitors. We found the
268 degradation of p65 induced by Vangl2 was blocked by autolysosome inhibitor
269 chloroquine (CQ) and bafilomycin A1 (Baf A1), or autophagy inhibitor 3-methyladenine
270 (3-MA) (Fig. 4 E), but not by the proteasome inhibitor MG132 or caspase-1 inhibitor Z-
271 VAD and VX-765 (Fig. 4 E and Fig. S4 C). Furthermore, Vangl2 significantly increased
272 the degradation of p65 during rapamycin-triggered autophagy (Fig. 4 F), which
273 suggested that Vangl2 promoted autophagic degradation of p65.
274 To further demonstrate Vangl2 mediated p65 degradation through autophagy, we
275 transfected WT, ATG5, and Beclin1 knockout (KO) 293T cells with Vangl2, and found
276 that the degradation of p65 triggered by Vangl2 was almost abrogated in ATG5 and
277 Beclin1 KO cells (Fig. 4 G). The p65 turnover rates were markedly reduced in ATG5 and
278 Beclin1 KO cells post CHX treatment (Fig. S4, D and E), suggesting that the impaired
279 autophagy prevented p65 degradation. Consistently, NF-κB activation induced by p65
280 was rescued in ATG5 and Beclin1 KO cells expressing Vangl2, compared to WT 293T
281 cells (Fig. 4, H and I). Together, our data suggest that Vangl2 specifically promotes p65
282 degradation through autophagy.
283
284 **Vangl2 promotes the recognition of p65 by cargo receptor NDP52.**
285 Accumulating evidence showed that cargo receptors play crucial roles in selective
286 autophagic degradation by delivering substrates (X. He et al., 2019; Kirkin & Rogov,
287 2019; Wu et al., 2021). Since there is no research suggests that Vangl2 is a cargo
288 protein, we hypothesized that Vangl2 might bridge p65 to the cargo receptors for
289 autophagic degradation. To identify the potential cargo receptor responsible for Vangl2-
290 mediated autophagic degradation of p65, we co-transfected 293T cells with Vangl2 and
291 various cargo receptors, followed by Co-IP assay. Result suggested that Vangl2 strongly
292 interacted with the cargo receptors p62 and NDP52, and slightly associated with NBR1
293 and Nix (Fig. 5 A). However, p65 only interacted with the cargo receptors p62 and
294 NDP52 (Fig. 5 B), which is consistent with a recent finding that p62 protein is a Vangl2-
295 binding partner (Puvirajesinghe et al., 2016). We next attempted to clarify whether p62
296 or NDP52 is involved in Vangl2-mediated autophagic degradation of p65. Interestingly,

297 we found that Vangl2 promoted the association between p65 and NDP52, but did not
298 affect p65-p62 complex (Fig. 5 C). Consistently, we found that Vangl2 mediated
299 degradation of p65 was rescued in NDP52 KO cells, but not in p62 KO cells (Fig. 5 D).
300 Endogenous co-IP immunoblot analyses also revealed that deficiency of Vangl2
301 remarkably attenuated the association of endogenous p65 and NDP52 (Fig. 5 E).
302 Likewise, NDP52, but not p62, enhanced the association between p65 and Vangl2 (Fig.
303 5 F and Fig. S5 A). And Vangl2 failed to inhibit the activation of NF-κB signaling in
304 NDP52 KO cells (Fig. 5 G), but not in p62 KO cells (Fig. S5 B). Furthermore, compared
305 with WT cells, CHX-chase assay results showed that the degradation rates of p65 were
306 reduced in NDP52 KO cells (Fig. 5 H), but not in p62 KO cells (Fig. S5 C). Taken
307 together, these data suggest that Vangl2 mediates the NDP52-directed selective
308 autophagic degradation of p65.
309
310 **Vangl2 increases the K63-linked poly-ubiquitination of p65.**
311 It has been well documented that ubiquitin chains attached to the substrates and served
312 as a signal for the recognition by cargo receptors (Otten et al., 2021; Shaid, Brandts,
313 Serve, & Dikic, 2013; Yin, Popelka, Lei, Yang, & Klionsky, 2020). The ubiquitin-
314 associated (UBA) domain of NDP52 mostly recognized ubiquitinated substrates for
315 degradation through autophagy (Johansen & Lamark, 2014; Yamano & Youle, 2020).
316 We hypothesized that Vangl2 may affect the ubiquitin chains on p65 for subsequent
317 NDP52-dependent degradation. To demonstrate this, we performed endogenous co-IP
318 assay and found that the poly-ubiquitination of p65 was impaired in BMDMs from
319 *Vangl2*$^{\Delta M}$ mice after LPS stimulation, compared to WT mice (Fig. 6 A). Moreover,
320 Vangl2 specifically increased K63-linked (K63-only ubiquitin mutant) poly-ubiquitination
321 of p65 (Fig. 6 B), but not other ubiquitin linkages (K11, K27, K33, or K48-only ubiquitin
322 mutant) in an overexpression system (Fig. 6 C). To further confirm that Vangl2 mediated
323 K63-linked poly-ubiquitinated p65, we knocked down Vangl2 by siRNA and found that
324 the absence of Vangl2 inhibited K63-linked poly-ubiquitination of p65 (Fig. 6 D).
325 Together, these results suggest that Vangl2 promotes the degradation of p65 by
326 promoting the K63-linked ubiquitination of p65.
327
328 **Vangl2 recruits PDLIM2 to ubiquitinate p65.**
329 Although Vangl2 promotes K63-linked ubiquitination and degradation of p65, Vangl2 is
330 not an E3 ubiquitin ligase. We hypothesized that Vangl2 might function as a scaffold

331 protein to link p65 and its E3 ubiquitin ligase for ubiquitination or to block the interaction
332 of deubiquitinase (DUB) with p65. To identify the potential E3 ubiquitinase or DUB
333 responsible for Vangl2 mediated ubiquitination of p65, we further analyzed our RNA-seq
334 data to identify E3 ubiquitin ligase or DUB involved in ubiquitination of p65 by comparing
335 LPS-stimulated BMDMs from *Vangl2*$^{\Delta M}$ and WT mice. Differentially expression analysis
336 identified 88 down-regulated genes related to E3 ubiquitin ligase and 56 up-regulated
337 genes related to DUB in response to Vangl2 deficiency in BMDMs after LPS stimulation
338 (Fig. S6 A), which included PDZ-LIM domain-containing protein 2 (PDLIM2), Trim21 and
339 DUB ubiquitin-specific peptidase 7 (USP7). Recent research showed that ubiquitin E3
340 ligases PDLIM2 and Trim21 ubiquitinated p65 via K63 linkage and enhanced the
341 interaction of p65 with IKK (Healy & O'Connor, 2009; Jodo, Shibazaki, Onuma, Kaisho,
342 & Tanaka, 2020; Yang et al., 2021), while DUB USP7 promoted NF-κB-mediated
343 transcription (Mitxitorena et al., 2020). Here, we found that the mRNA level of PDLIM2
344 and USP7 decreased in Vangl2-deficient BMDMs, compared with WT BMDMs (Fig. S6,
345 B-D). To investigate which E3 ubiquitin ligase or DUB is recruited by Vangl2, luciferase
346 assay in Vangl2-expressing 293T cells transfected with scramble, *Pdlim2*, *Usp7*, or
347 *Trim21* siRNA (Fig. S6, E-G) suggested Vangl2-mediated inhibition of NF-κB activation
348 and degradation of p65 were blocked by knocking down PDLIM2, but not USP7 or
349 Trim21 (Fig. 7 A). Meanwhile, *Pdlim2* knockdown in BMDMs also resulted in higher
350 expression of *Il6* and *Il1b* in response to LPS stimulation (Fig. 7, B and C), indicating that
351 PDLIM2 plays a key role in promoting Vangl2-mediated p65 degradation.
352 We next investigated whether Vangl2 promoted the association between p65 and
353 PDLIM2 by co-IP experiments. Our results indicated that Vangl2 interacted with PDLIM2
354 (Fig. 7 D) and promoted the association between p65 and PDLIM2 (Fig. 7 E). Notably,
355 PDLIM2 accelerated the degradation of p65 in the presence of Vangl2 (Fig. 7 F).
356 Conversely, PDLIM2 deficiency markedly impaired Vangl2-mediated K63-linked
357 ubiquitination of p65 (Fig. 7 G) and knockdown of Vangl2 inhibited K63-linked poly-
358 ubiquitination of p65 mediated by PDLIM2 (Fig. 7 H). Taken together, these data
359 suggest that Vangl2 functions as a potential adaptor to recruit E3 ubiquitin ligase
360 PDLIM2 to p65 and promotes the K63-linked ubiquitination of p65 for its subsequent
361 autophagic degradation.
362
363 **Discussion**

364 As a core PCP component, Vangl2 is widely known for its function in organ development,
365 such as brain, tooth, tongue and kidney (Bailly et al., 2018; Hatakeyama et al., 2014),
366 trafficking from the endoplasmic reticulum (ER) to the cell surface, and subsequently
367 shuttles between the endocytic vesicles and cell surface (D. Feng et al., 2021). The
368 function of Vangl2 mostly depends on its cellular localization (Hatakeyama et al., 2014)
369 and is reported mainly through PCP/WNT signaling pathway (Jessen & Jessen, 2019).
370 Activated Vangl2 exhibits extremely long cytoplasmic and intercellular branches and
371 delivers Wnt to multiple cells to enhance Wnt/β-Catenin signaling (Brunt et al., 2021).
372 During myocardial hypertrophy, Vangl2 aggravates myocardial hypertrophy by regulating
373 Wnt/JNK signaling (Brunt et al., 2021; Jessen & Jessen, 2017, 2019) and the expansion
374 of cardiomyocyte surface area (Brunt et al., 2021; Jessen & Jessen, 2017, 2019).
375 However, our previous study showed that the lysosome-suppressing function of Vangl2
376 in osteoblast differentiation is not dependent on conventional PCP pathway (Gong et al.,
377 2021), suggesting that Vangl2 has additional functions in pathways besides PCP. In this
378 study, we provided direct evidence that the expression of Vangl2 was increased during
379 sepsis and upregulated significantly in immune organs (lymph nodes and spleen) upon
380 LPS stimulation, which is consistent with our previous finding that Vangl2 regulated the
381 downstream signaling of TLR or IL-1R. In addition, the present study showed that
382 Vangl2 prevented the progression of sepsis and the accumulation of inflammatory
383 cytokines through suppressing NF-κB pathway: Vangl2 inhibited LPS-induced NF-κB
384 activation by delivering p65 to autophagosome for degradation. To the best of our
385 knowledge, this is the first study proves that Vangl2 regulates NF-κB signaling and
386 inflammatory responses, and could serve as a potential target for therapeutic purposes
387 in diseases associated with NF-κB signaling.

388 The proteasome, lysosome and autolysosome pathways are the major systems that
389 are utilized by eukaryotic cells to maintain the protein abundance and immune
390 homeostasis (Deretic, 2021). Previous studies have shown that cellular levels of Vangl2
391 (D. Feng et al., 2021) and its binding partner Prickle2 (Nagaoka et al., 2019) are
392 maintained by the proteasomal pathway. Our recent study showed that Vangl2 mediated
393 osteogenic differentiation by limiting chaperone-mediated autophagy (CMA) in
394 mesenchymal stem cells, suggesting a close relationship between Vangl2 and
395 autophagy (Gong et al., 2021). Indeed, our study suggests Vangl2 promotes p65
396 degradation through autophagy pathway, but not proteasomal pathway. Importantly, we
397 demonstrated that the degradation of p65 mediated by Vangl2-NDP52 complex is

398 regulated by autophagy induction through rapamycin treatment and autophagy blockade
399 by ATG5 KO or Beclin1 KO. Considering our findings and other reports, Vangl2 may
400 play multi-functional roles in regulating different types of autophagy (i.e. CMA or
401 selective autophagy).

402 Selective autophagy requires that cargo receptors recognize the labeling of cargoes
403 with degradation signals and subsequently engaged with the LC3 localized in the
404 autophagosome membrane (Shaid et al., 2013). Common cargo receptors mainly
405 include p62/SQSTM1, CALCOCO2/NDP52, OPTN, NBR1 and TOLLIP (Johansen &
406 Lamark, 2014; Yamano & Youle, 2020). A study in HEK293T cells showed that LRRC25
407 promotes the autophagic degradation of p65 through enhancing the interaction between
408 p65 and p62 (Y. Feng et al., 2017). In addition, a recent study showed that Vangl2
409 interacts with p62, subsequently promoting breast tumors by activating JNK signaling
410 (Puvirajesinghe et al., 2016). Thus, we hypothesized that Vangl2 may promote the
411 autophagic degradation of p65 by recruiting the cargo receptor p62. However, our data
412 suggested that Vangl2 markedly increased the p65-NDP52 interaction but not p65-p62.
413 Strikingly, Vangl2 mediated autophagic degradation of p65 was abolished in NDP52 KO
414 cells, but not in p62 KO cells. Thus, our findings identify that NDP52 is the new cargo
415 receptor responsible for Vangl2-mediated selective autophagic degradation of p65.

416 Accumulating evidence has shown that cargo receptors mainly recognize
417 ubiquitination modifications on the substrates and then promote degradation in auto-
418 lysosome (Shaid et al., 2013). As expected, we observed Vangl2 promoted the
419 ubiquitination of p65, thus enhancing the association between cargo protein and p65.
420 K48- and K63-linked ubiquitination were mostly reported modifications on p65
421 (Kauppinen, Suuronen, Ojala, Kaarniranta, & Salminen, 2013; Korbecki, Bobinski, &
422 Dutka, 2019). For example, E3 ubiquitin ligase RNF182 inhibited TLR triggered cytokine
423 production by promoting K48-linked poly-ubiquitination of p65 (Cao, Sun, Chang, Sun, &
424 Yang, 2019). Trim21 promoted K63-linked poly-ubiquitination of p65, but did not affect
425 the stability of p65 (Yang et al., 2021). PDLIM7 cooperated with PDLIM2 to inhibit
426 inflammation by promoting K63-linked poly-ubiquitination of p65 (Jodo et al., 2020). In
427 this study, we revealed that Vangl2 specifically promoted K63-linked poly-ubiquitination
428 of p65, but not other ubiquitin linkages by recruiting a previously unrecognized E3 ligase
429 PDLIM2, which further explore the molecular mechanism by which regulates the stability
430 of p65.–Although many studies focus on the regulation of p65, the location of p65
431 degradation has not been clarified. A study showed PDLIM2 degrades p65 through the

proteasomal pathway in the nucleus (Jodo et al., 2020), while we found Vangl2 mediated autophagic degradation of p65 mainly happened in cytoplasm, but not in nucleus. Combined with previous studies, our study indicates that p65 undergoes different degradation pathway in distinct location of cells.

Autophagy is a fundamental biological process contributing to multiple life processes. Emerging evidence has suggested that crosstalk between autophagy and innate immune signaling plays critical roles in diseases with inflammatory components, including infections, cancer, autoimmunity, and metabolic disorders (Pradel et al., 2020; Wu et al., 2021). Recent study showed that the interplay between autophagy and type I IFN or NF-κB signaling drives or suppresses inflammatory responses during SARS-CoV-2 infection (Hui et al., 2021). Moreover, autophagy related key genes, such as Atg5, Atg9, and ULK1, also play critical roles in inflammatory diseases (Y. He et al., 2018; Peng et al., 2019). Here, our discovery of Vangl2-PDLIM2-NDP52 complex in the regulation of p65-mediated NF-κB signaling could be a therapeutic target for the development of immunotherapy against infection and inflammation.

Based on our findings, we propose a working model that Vangl2 negatively regulates NF-κB signaling (Fig. 7 I). Vangl2 functions as an adaptor to recruit ubiquitin ligase PDLIM2 and increase K63-linked ubiquitination on p65, which promotes the recognition of p65 by cargo receptor NDP52 and the autophagic degradation of p65, resulting in suppressing the production of pro-inflammatory cytokines and ameliorating sepsis. Our findings provide a potential target for the treatment of inflammatory diseases.

Materials and Methods

Animal and sepsis model

All animal experiments were approved by the Southern Medical University Animal Care and Use Committee (SMUL20201010). The *Vangl2*$^{flox/flox}$ mice and lysozyme-Cre (*Lyz2*-Cre) mice were obtained from the Jackson Laboratory (Bar Harbor, ME, USA; Jax no. 025174 and 004781, respectively). *Vangl2*$^{flox/flox}$ mice were hybridized with *Lyz2*-Cre mice to obtain *Vangl2*$^{flox/flox}$*Lyz2*-Cre (*Vangl2*$^{\Delta M}$) mice with *Vangl2* specific deficiency in myeloid cells. Co-housed littermate controls with normal *Vangl2* expression were used as wild type (WT). For sepsis model, 10-weeks-old mice were intraperitoneally (i.p.) injected with LPS (25-30 mg/kg), and survival rate of mice was continuously observed.

466 For other detection, mice with sepsis were sacrificed and samples were collected at
467 indicated time points.
468
469 **Isolation of immune cells**
470 For bone marrow (BM)-derived macrophages (BMDMs), BM cells were collected from
471 the femur and tibia, and then maintained in 20% L929 conditioned media with 1%
472 penicillin-streptomycin and macrophage-colony stimulating factor (M-CSF) (St Louis,
473 MO, USA) for 6 days, as previously described(Tan et al., 2019). Mouse peritoneal
474 macrophages were acquired from ascites of indicated mice, which were administrated
475 intraperitoneally (i.p.) with 4% (v/v) thioglycollate (BD) for three consecutive days before
476 sacrifice. As for primary neutrophils, mice were administrated (i.p.) with 4% (v/v)
477 thioglycollate (BD) for 4 h before sacrifice. Peritoneal cavities were flushed with PBS to
478 obtain peritoneal macrophages or neutrophils. Cells were cultured in complete DMEM
479 (Corning) supplemented with 100 U/ml penicillin (Sigma), 100 μg/ml streptomycin
480 (Sigma) and 10% FBS (HyClone) for 6 h and then washed twice with PBS to remove
481 adherent cells. For human PBMC isolation, 4 ml of whole blood was harvested from
482 each sepsis patient and healthy control. The white membrane layer was collected after
483 density gradient centrifugation at 400 g for 25 min and the PBMCs were filtered and
484 prepared for the subsequent experiments after the removal of the red blood cells. For
485 mouse $CD11b^+$ splenocytes isolation, spleens were digested in 2% FBS-DMEM with
486 200 U/ml DNase I (Sigma, USA) and 1 mg/ml collagenase type II (Sigma, USA) at 37 °C
487 for 30 min. Then tissues digested were filtered through a 70 μm cell strainer and red cells
488 were removed by ACK. The rest splenocytes were labeled with anti-mouse CD11b biotin
489 antibodies (Biolegend). The mixture above was then incubated with streptavidin-
490 paramagnetic particles (BD Biosciences) at 4 °C for 30 min. Purification of $CD11b^+$
491 splenocytes was performed by DynaMag™ (Thermo Fisher Science). Isolated cells
492 achieved a purity of ≥95% measured by FACS.
493
494 **Cell isolation and culture**
495 HEK293T, A549, CHO and Raw 264.7 cells were obtained from the American Type
496 Culture Collection (ATCC). Above cell lines were maintained in complete DMEM,
497 supplemented with 10% FBS, 100 U/ml penicillin and streptomycin. All cells were
498 cultured at 37 °C with 5% CO_2.
499

500 **Cell treatment**

501 To test cytokines expression and signaling pathway activation, BMDMs, neutrophils and
502 A549 cells were treated with LPS (200 ng/ml) for the indicated time. For dual luciferase
503 assay, HEK293T cells were treated with LPS (250 ng/ml), IL-1β (40 ng/ml) or TNF-α (20
504 ng/ml) for 6 h. For protein degradation inhibition assays in HEK293T cells, CQ (50 μM),
505 3MA (10 mM), or bafilomycin A1 (Baf A1) (0.2 μM) was used to inhibit autolysosome- or
506 lysosome-mediated protein degradation. MG132 (10 μM) was used to inhibit
507 proteasome-mediated protein degradation. Z-VAD-FMK (50 μM) was used to inhibit
508 Caspase-mediated protein degradation.

509

510 **Luciferase and reporter assays**

511 HEK293T cells were plated in 24-well plates and transfected with pRL-TK and plasmids
512 encoding the NF-κB luciferase reporter, together with different plasmids following: Flag-
513 MyD88, Flag-IRAK1, Flag-TRAF6, Flag-IKKα, Flag-IKKβ, Flag-p65 and an increasing
514 doses of the HA-Vangl2 vector (250, 500, 1000 ng) or empty vector. In addition, CHO or
515 HEK293T cells were administrated with or without LPS (1000 ng/ml), IL-1β (1000 ng/ml)
516 or TNF-α (100 ng/ml) for 6-8 h after transfection with pRL-TK and plasmids encoding the
517 NF-κB luciferase reporter. Then, cells were collected at 24 h post-transfection and
518 luciferase activity was analyzed by Dual-Luciferase Reporter Assay Kit (Vazyme)
519 performed with a Luminoskan Ascent luminometer (Thermo Fisher Scientific). The
520 activity of Firefly luciferase was normalized by that of Renilla luciferase to obtain relative
521 luciferase activity.

522

523 **Enzyme-linked immunosorbent assay (ELISA)**

524 IL-1β, IL-6 and TNF-α in cell supernatants and mice serum were measured using ELISA
525 kit (#E-EL-M0037c, #E-EL-M0044c, #E-EL-M1084c, respectively; Elabscience
526 Biotechnology) following the manufacturer's instructions. Absorbance was detected at
527 450 nm by the Multiscan FC (Thermo Fisher, Waltham, MA, USA).

528

529 **Statistical Analysis**

530 The data of all quantitative experiments are presented as mean ± SD of at least three
531 independent experiments. Curve data was assessed by GraphPad Prism 8.0 (USA). And

532 comparisons between groups for statistically significant differences were analyzed with a
533 two-tailed Student's t test. The statistical significance was defined as $p < 0.05$.
534
535 **Online supplemental material**
536 Fig. S1 shows that the expression of Vangl2 during sepsis and LPS treatment. Fig. S2
537 shows that Vangl2 defection promotes LPS-induced NF-κB activation and production of
538 inflammatory cytokines. Fig. S3 shows that Vangl2 interacts with p65 to inhibit NF-κB
539 activation. Fig. S4 shows that Vangl2 promotes p65 degradation by autophagic pathway.
540 Fig. S5 shows that Vangl2 promoted autophagic degradation of p65 is not mediated by
541 cargo receptor p62. Fig. S6 shows that Expression of candidate E3 ubiquitin ligases in
542 WT and Vangl2-deficient BMDMs after LPS treatment. Table S1 shows Reagents and
543 antibodies used in this study. Table S2 shows Primers sequences for quantitative RT-
544 PCR.
545
546 **Acknowledgments**
547 We thank Dr. Jun Cui (Sun Yat-sen University) for providing ATG5, Beclin1, NDP52 and
548 p62 KO HEK293T cells. This work was supported by grants from National Natural
549 Science Foundation of China (82171741 and 81801579), the Science and Technology
550 Planning Project of Guangzhou (201904010064), Guangdong Zhujiang Youth Scholar
551 funding, Guangdong Basic and Applied Basic Research Foundation (2019B1515120033
552 and 2021A1515012140), and the Start-up Fund for High-level Talents of Southern
553 Medical University.
554
555 **Author Contributions:** J.L., J.Z., H.J. and Z.H. designed and performed the
556 experiments. L.H., D.W., K.Z., P.T., and Z.G. provided assistance or technical support in
557 some experiments. H. L., Y. X., J. Y., Q. X. and Z. S. collected samples. J. L. performed
558 statistical analysis. J.L., J.Z., Z.H., X.B. and X.Y. performed data analysis and wrote the
559 manuscript. X.Y. supervised the entire project.
560
561 **References**
562 Ashrafi, G., & Schwarz, T. L. (2013). The pathways of mitophagy for quality control and clearance
563 of mitochondria. *Cell Death Differ, 20*(1), 31-42. doi:10.1038/cdd.2012.81
564 Bailly, E., Walton, A., & Borg, J. P. (2018). The planar cell polarity Vangl2 protein: From genetics
565 to cellular and molecular functions. *Semin Cell Dev Biol, 81*, 62-70.

566 doi:10.1016/j.semcdb.2017.10.030
567 Bartuzi, P., Hofker, M. H., & van de Sluis, B. (2013). Tuning NF-kappaB activity: a touch of
568 COMMD proteins. *Biochim Biophys Acta, 1832*(12), 2315-2321. doi:10.1016/j.bbadis.2013.09.014
569 Brunt, L., Greicius, G., Rogers, S., Evans, B. D., Virshup, D. M., Wedgwood, K. C. A., & Scholpp,
570 S. (2021). Vangl2 promotes the formation of long cytonemes to enable distant Wnt/beta-catenin
571 signaling. *Nat Commun, 12*(1), 2058. doi:10.1038/s41467-021-22393-9
572 Cancer Genome Atlas Research, N., Kandoth, C., Schultz, N., Cherniack, A. D., Akbani, R., Liu,
573 Y., . . . Levine, D. A. (2013). Integrated genomic characterization of endometrial carcinoma.
574 *Nature, 497*(7447), 67-73. doi:10.1038/nature12113
575 Cao, Y., Sun, Y., Chang, H., Sun, X., & Yang, S. (2019). The E3 ubiquitin ligase RNF182 inhibits
576 TLR-triggered cytokine production through promoting p65 ubiquitination and degradation. *FEBS*
577 *Lett, 593*(22), 3210-3219. doi:10.1002/1873-3468.13583
578 Cartwright, T., Perkins, N. D., & C, L. W. (2016). NFKB1: a suppressor of inflammation, ageing
579 and cancer. *FEBS J, 283*(10), 1812-1822. doi:10.1111/febs.13627
580 Cerami, E., Gao, J., Dogrusoz, U., Gross, B. E., Sumer, S. O., Aksoy, B. A., . . . Schultz, N.
581 (2012). The cBio cancer genomics portal: an open platform for exploring multidimensional cancer
582 genomics data. *Cancer Discov, 2*(5), 401-404. doi:10.1158/2159-8290.CD-12-0095
583 Cui, J., Zhu, L., Xia, X., Wang, H. Y., Legras, X., Hong, J., . . . Wang, R. F. (2010). NLRC5
584 negatively regulates the NF-kappaB and type I interferon signaling pathways. *Cell, 141*(3), 483-
585 496. doi:10.1016/j.cell.2010.03.040
586 Denton, D., & Kumar, S. (2019). Autophagy-dependent cell death. *Cell Death Differ, 26*(4), 605-
587 616. doi:10.1038/s41418-018-0252-y
588 Deretic, V. (2021). Autophagy in inflammation, infection, and immunometabolism. *Immunity,*
589 *54*(3), 437-453. doi:10.1016/j.immuni.2021.01.018
590 Feng, D., Wang, J., Yang, W., Li, J. Y., Lin, X. C., Zha, F. Z., . . . Gao, B. (2021). Regulation of
591 Wnt/PCP signaling through p97/VCP-KBTBD7-mediated Vangl ubiquitination and endoplasmic
592 reticulum-associated degradation. *SCIENCE ADVANCES, 7*(20). doi:ARTN eabg2099
593 10.1126/sciadv.abg2099
594 Feng, Y., Duan, T., Du, Y., Jin, S., Wang, M., Cui, J., & Wang, R. F. (2017). LRRC25 Functions
595 as an Inhibitor of NF-kappaB Signaling Pathway by Promoting p65/RelA for Autophagic
596 Degradation. *Sci Rep, 7*(1), 13448. doi:10.1038/s41598-017-12573-3
597 Funes, S. C., Rios, M., Escobar-Vera, J., & Kalergis, A. M. (2018). Implications of macrophage
598 polarization in autoimmunity. *Immunology, 154*(2), 186-195. doi:10.1111/imm.12910
599 Gao, J., Aksoy, B. A., Dogrusoz, U., Dresdner, G., Gross, B., Sumer, S. O., . . . Schultz, N.
600 (2013). Integrative analysis of complex cancer genomics and clinical profiles using the cBioPortal.
601 *Sci Signal, 6*(269), pl1. doi:10.1126/scisignal.2004088
602 Gatica, D., Lahiri, V., & Klionsky, D. J. (2018). Cargo recognition and degradation by selective

603 autophagy. *Nat Cell Biol, 20*(3), 233-242. doi:10.1038/s41556-018-0037-z
604 Gong, Y., Li, Z., Zou, S., Deng, D., Lai, P., Hu, H., . . . Zou, Z. (2021). Vangl2 limits chaperone-
605 mediated autophagy to balance osteogenic differentiation in mesenchymal stem cells. *Dev Cell,*
606 *56*(14), 2103-2120 e2109. doi:10.1016/j.devcel.2021.06.011
607 Hatakeyama, J., Wald, J. H., Printsev, I., Ho, H. Y., & Carraway, K. L., 3rd. (2014). Vangl1 and
608 Vangl2: planar cell polarity components with a developing role in cancer. *Endocr Relat Cancer,*
609 *21*(5), R345-356. doi:10.1530/ERC-14-0141
610 He, X., Zhu, Y., Zhang, Y., Geng, Y., Gong, J., Geng, J., . . . Zhong, H. (2019). RNF34 functions
611 in immunity and selective mitophagy by targeting MAVS for autophagic degradation. *EMBO J,*
612 *38*(14), e100978. doi:10.15252/embj.2018100978
613 He, Y., She, H., Zhang, T., Xu, H., Cheng, L., Yepes, M., . . . Mao, Z. (2018). p38 MAPK inhibits
614 autophagy and promotes microglial inflammatory responses by phosphorylating ULK1. *J Cell Biol,*
615 *217*(1), 315-328. doi:10.1083/jcb.201701049
616 Healy, N. C., & O'Connor, R. (2009). Sequestration of PDLIM2 in the cytoplasm of
617 monocytic/macrophage cells is associated with adhesion and increased nuclear activity of NF-
618 kappaB. *J Leukoc Biol, 85*(3), 481-490. doi:10.1189/jlb.0408238
619 Hui, X., Zhang, L., Cao, L., Huang, K., Zhao, Y., Zhang, Y., . . . Jin, M. (2021). SARS-CoV-2
620 promote autophagy to suppress type I interferon response. *Signal Transduct Target Ther, 6*(1),
621 180. doi:10.1038/s41392-021-00574-8
622 Jessen, T. N., & Jessen, J. R. (2017). VANGL2 interacts with integrin alphav to regulate matrix
623 metalloproteinase activity and cell adhesion to the extracellular matrix. *Exp Cell Res, 361*(2), 265-
624 276. doi:10.1016/j.yexcr.2017.10.026
625 Jessen, T. N., & Jessen, J. R. (2019). VANGL2 protein stability is regulated by integrin alphav
626 and the extracellular matrix. *Exp Cell Res, 374*(1), 128-139. doi:10.1016/j.yexcr.2018.11.017
627 Jodo, A., Shibazaki, A., Onuma, A., Kaisho, T., & Tanaka, T. (2020). PDLIM7 Synergizes With
628 PDLIM2 and p62/Sqstm1 to Inhibit Inflammatory Signaling by Promoting Degradation of the p65
629 Subunit of NF-kappaB. *Front Immunol, 11*, 1559. doi:10.3389/fimmu.2020.01559
630 Johansen, T., & Lamark, T. (2014). Selective autophagy mediated by autophagic adapter
631 proteins. *Autophagy, 7*(3), 279-296. doi:10.4161/auto.7.3.14487
632 Kauppinen, A., Suuronen, T., Ojala, J., Kaarniranta, K., & Salminen, A. (2013). Antagonistic
633 crosstalk between NF-kappaB and SIRT1 in the regulation of inflammation and metabolic
634 disorders. *Cell Signal, 25*(10), 1939-1948. doi:10.1016/j.cellsig.2013.06.007
635 Kirkin, V., & Rogov, V. V. (2019). A Diversity of Selective Autophagy Receptors Determines the
636 Specificity of the Autophagy Pathway. *Mol Cell, 76*(2), 268-285. doi:10.1016/j.molcel.2019.09.005
637 Korbecki, J., Bobinski, R., & Dutka, M. (2019). Self-regulation of the inflammatory response by
638 peroxisome proliferator-activated receptors. *Inflamm Res, 68*(6), 443-458. doi:10.1007/s00011-
639 019-01231-1

640 Liu, T., Zhang, L., Joo, D., & Sun, S. C. (2017). NF-kappaB signaling in inflammation. *Signal*
641 *Transduct Target Ther, 2*. doi:10.1038/sigtrans.2017.23
642 Locati, M., Curtale, G., & Mantovani, A. (2020). Diversity, Mechanisms, and Significance of
643 Macrophage Plasticity. *Annu Rev Pathol, 15*, 123-147. doi:10.1146/annurev-pathmechdis-
644 012418-012718
645 Mao, X., Gluck, N., Li, D., Maine, G. N., Li, H., Zaidi, I. W., . . . Burstein, E. (2009). GCN5 is a
646 required cofactor for a ubiquitin ligase that targets NF-kappaB/RelA. *Genes Dev, 23*(7), 849-861.
647 doi:10.1101/gad.1748409
648 Mitxitorena, I., Somma, D., Mitchell, J. P., Lepisto, M., Tyrchan, C., Smith, E. L., . . . Carmody, R.
649 J. (2020). The deubiquitinase USP7 uses a distinct ubiquitin-like domain to deubiquitinate NF-kB
650 subunits. *J Biol Chem, 295*(33), 11754-11763. doi:10.1074/jbc.RA120.014113
651 Nagaoka, T., Furuse, M., Ohtsuka, T., Tsuchida, K., & Kishi, M. (2019). Vangl2 interaction plays a
652 role in the proteasomal degradation of Prickle2. *Sci Rep, 9*(1), 2912. doi:10.1038/s41598-019-
653 39642-z
654 Otten, E. G., Werner, E., Crespillo-Casado, A., Boyle, K. B., Dharamdasani, V., Pathe, C., . . .
655 Randow, F. (2021). Ubiquitylation of lipopolysaccharide by RNF213 during bacterial infection.
656 *Nature, 594*(7861), 111-116. doi:10.1038/s41586-021-03566-4
657 Papakrivopoulou, E., Vasilopoulou, E., Lindenmeyer, M. T., Pacheco, S., Brzoska, H. L., Price, K.
658 L., . . . Long, D. A. (2018). Vangl2, a planar cell polarity molecule, is implicated in irreversible and
659 reversible kidney glomerular injury. *J Pathol, 246*(4), 485-496. doi:10.1002/path.5158
660 Peng, X., Wang, Y., Li, H., Fan, J., Shen, J., Yu, X., . . . Mao, H. (2019). ATG5-mediated
661 autophagy suppresses NF-kappaB signaling to limit epithelial inflammatory response to kidney
662 injury. *Cell Death Dis, 10*(4), 253. doi:10.1038/s41419-019-1483-7
663 Poobalasingam, T., Yates, L. L., Walker, S. A., Pereira, M., Gross, N. Y., Ali, A., . . . Dean, C. H.
664 (2017). Heterozygous Vangl2(Looptail) mice reveal novel roles for the planar cell polarity pathway
665 in adult lung homeostasis and repair. *Dis Model Mech, 10*(4), 409-423. doi:10.1242/dmm.028175
666 Pradel, B., Robert-Hebmann, V., & Espert, L. (2020). Regulation of Innate Immune Responses by
667 Autophagy: A Goldmine for Viruses. *Front Immunol, 11*, 578038. doi:10.3389/fimmu.2020.578038
668 Puvirajesinghe, T. M., Bertucci, F., Jain, A., Scerbo, P., Belotti, E., Audebert, S., . . . Borg, J. P.
669 (2016). Identification of p62/SQSTM1 as a component of non-canonical Wnt VANGL2-JNK
670 signalling in breast cancer. *Nat Commun, 7*, 10318. doi:10.1038/ncomms10318
671 Shaid, S., Brandts, C. H., Serve, H., & Dikic, I. (2013). Ubiquitination and selective autophagy.
672 *Cell Death Differ, 20*(1), 21-30. doi:10.1038/cdd.2012.72
673 Tan, P., He, L., Xing, C., Mao, J., Yu, X., Zhu, M., . . . Wang, R. F. (2019). Myeloid loss of Beclin
674 1 promotes PD-L1hi precursor B cell lymphoma development. *J Clin Invest, 129*(12), 5261-5277.
675 doi:10.1172/JCI127721
676 Tong, Y., Cui, J., Li, Q., Zou, J., Wang, H. Y., & Wang, R. F. (2012). Enhanced TLR-induced NF-

677 kappaB signaling and type I interferon responses in NLRC5 deficient mice. *Cell Res, 22*(5), 822-
678 835. doi:10.1038/cr.2012.53
679 Wu, Y., Jin, S., Liu, Q., Zhang, Y., Ma, L., Zhao, Z., . . . Cui, J. (2021). Selective autophagy
680 controls the stability of transcription factor IRF3 to balance type I interferon production and
681 immune suppression. *Autophagy, 17*(6), 1379-1392. doi:10.1080/15548627.2020.1761653
682 Yamano, K., & Youle, R. J. (2020). Two different axes CALCOCO2-RB1CC1 and OPTN-ATG9A
683 initiate PRKN-mediated mitophagy. *Autophagy, 16*(11), 2105-2107.
684 doi:10.1080/15548627.2020.1815457
685 Yang, L., Zhang, T., Zhang, C., Xiao, C., Bai, X., & Wang, G. (2021). Upregulated E3 ligase
686 tripartite motif-containing protein 21 in psoriatic epidermis ubiquitylates nuclear factor-kappaB p65
687 subunit and promotes inflammation in keratinocytes. *Br J Dermatol, 184*(1), 111-122.
688 doi:10.1111/bjd.19057
689 Yin, Z., Popelka, H., Lei, Y., Yang, Y., & Klionsky, D. J. (2020). The Roles of Ubiquitin in
690 Mediating Autophagy. *Cells, 9*(9). doi:10.3390/cells9092025
691
692

693 **Figures and Figure legends**

694

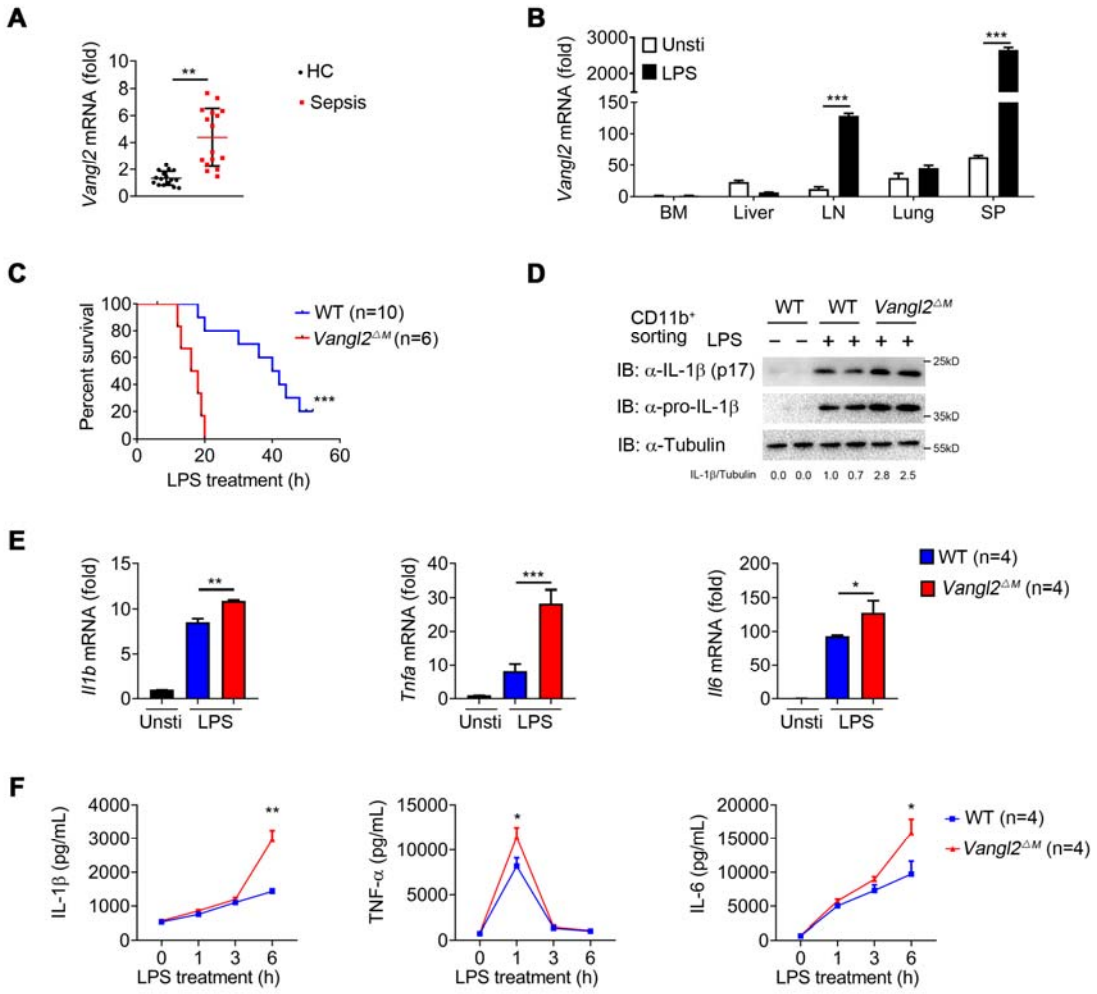

695

696

697 Figure 1. **Vangl2 ablation promotes inflammation during LPS treatment.**

698 **(A)** Transcription levels of *Vangl2* in PBMCs from healthy volunteers (healthy control,
699 HC) and sepsis patients were analyzed by real-time PCR (n≥4).

700 **(B)** *Vangl2* mRNA in different organs from mice treated with or without LPS (n≥3).

701 **(C)** The survival rates of WT and *Vangl2*$^{\Delta M}$ mice treated with high-dosage of LPS (30
702 mg/kg, i.p.) (n≥4).

703 **(D-F)** WT and *Vangl2*$^{\Delta M}$ mice (n≥3) were treated with LPS (30 mg/kg, i.p.). Splenocytes
704 were collected at 9 h after LPS treatment. Cell lysates of CD11b^{+} sorted splenocytes
705 were analyzed by immunoblotting with the indicated antibodies **(D)**. RNAs from
706 splenocytes were isolated and used for expression analysis of *Il1b*, *Tnfa*, and *Il6* using

707 qPCR **(E)**. Sera were collected at indicated times post LPS treatment and subjected to
708 ELISA analysis of IL-1β, TNF-α, and IL-6 **(F)**.
709 PBMCs, peripheral blood mononuclear cells; Unsti, unstimulation; LPS,
710 lipopolysaccharide; LN, lymph node; SP, spleen. Data are representative of three
711 independent experiments and are plotted as the mean ±SD. *$p<0.05$, **$p<0.01$,
712 ***$p<0.001$ vs. corresponding control.
713

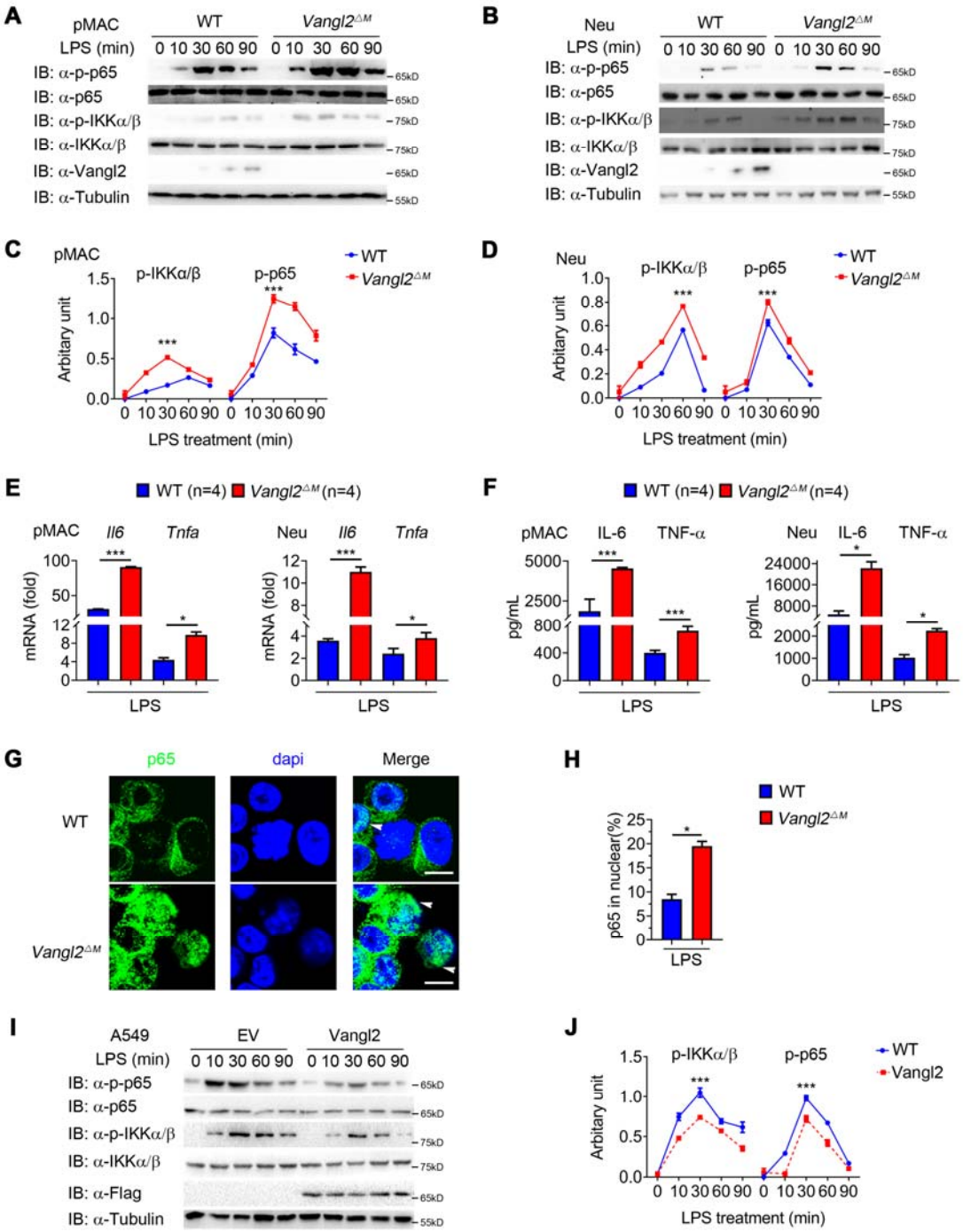

Figure 2. **Vangl2 negatively regulates LPS-induced NF-κB activation and proinflammatory cytokines.**

(A-D) WT and Vangl2-deficient (n≥3) pMAC **(A and C)** or neutrophils **(B and D)** were stimulated with LPS (100 ng/ml) for the indicated times. Immunoblot analysis of total and

720 phosphorylated p65, IKKα/β **(A and B)**, and analysis of grey intensity was shown **(C and**
721 **D)**.
722 **(E-F)** WT and Vangl2-deficient (n≥4) pMAC or neutrophils were stimulated with LPS
723 (100 ng/ml) for 6 h. mRNA levels of *Il6* and *Tnfa* were measure by qPCR **(E)**. IL-6 and
724 TNF-α secretion by WT and Vangl2-deficient BMDMs or neutrophils treated with or
725 without LPS for 6 h was measured by ELISA **(F)**.
726 **(G and H)** The WT and Vangl2-deficient (n≥3) neutrophils were treated with LPS (1000
727 ng/ml) for 4 h, and the nuclear translocation of p65 was detected by
728 immunofluorescence **(G)** (p65, green; DAPI, blue). Percentages of p65 nuclear
729 translocated cells in WT and Vangl2-deficient neutrophils were determined by counting
730 100 to 150 cells in non-overlapping fields **(H)**.
731 **(I and J)** A549 cells were transfected with Flag-tagged Vangl2 plasmid or empty vector,
732 then stimulated with LPS (100 ng/ml) for the indicated times. Immunoblot analysis of
733 total and phosphorylated p65, IKKα/β **(I)** (representative image), and analysis of grey
734 intensity was shown **(J)** (n≥3).
735 pMAC, peritoneal macrophage; Neu, neutrophil; EV, empty vector. Data are
736 representative of three independent experiments and are plotted as the mean ±SD.
737 *p<0.05, **p<0.01, ***p<0.001 vs. corresponding control.

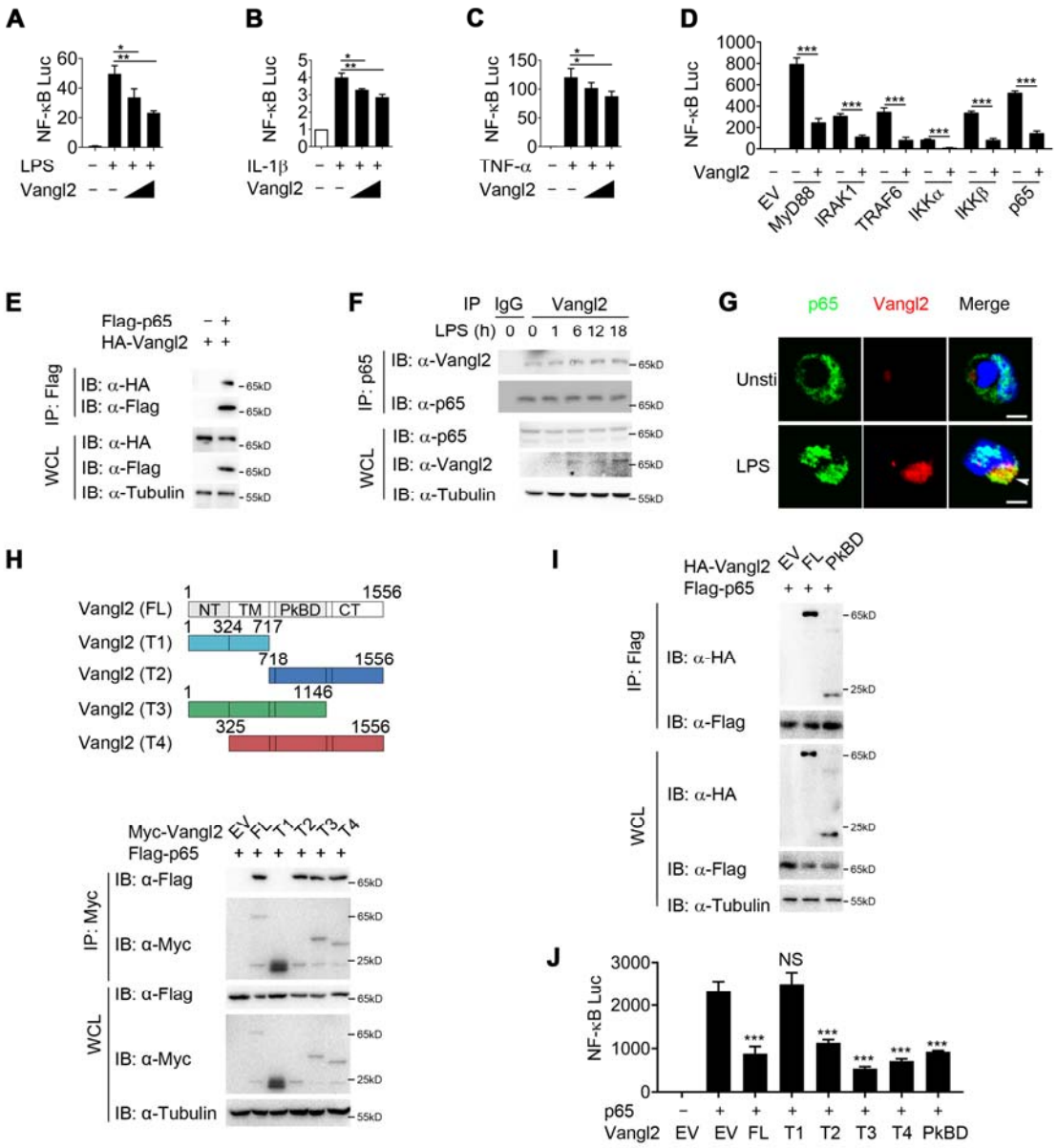

Figure 3. **Vangl2 inhibits NF-κB signaling by interacting with p65.**

(A-C) Cho **(A)** or HEK293T cells **(B and C)** were co-transfected with a NF-κB and TK-Renilla reporter along with increasing amounts of Vangl2 for 18 h, then treated the cells with or without LPS (A, 250ng/ml), IL-1β (B, 40 ng/ml), or TNF-α (C, 20 ng/ml) for 6 h. NF-κB promoter driven luciferase activity was measured and normalized to the Renilla luciferase activity.

(D) Luciferase activity in HEK293T transfected with plasmids encoding an NF-κB luciferase reporter and TK-Renilla reporter, together with a vector encoding MyD88,

748 IRAK1, TRAF6, IKKα, IKKβ, or p65, along with or without Vangl2 plasmid, was
749 measured at 24 h after transfection and normalized to the Renilla luciferase activity.
750 **(E)** HEK293T cells were transfected with plasmids encoding HA-tagged Vangl2 and
751 Flag-tagged p65, followed by immunoprecipitation with anti-Flag beads and immunoblot
752 analysis with anti-HA. Throughout was the immunoblot analysis of whole-cell lysates
753 without immunoprecipitation.
754 **(F)** BMDMs were stimulated with LPS (100 ng/ml) for the indicated times. The cell
755 lysates were subjected to immunoprecipitation with an anti-p65 antibody or control IgG,
756 followed by immunoblotting with an anti-Vangl2 or anti-p65 antibody.
757 **(G)** The WT and Vangl2-deficient peritoneal macrophages were treated with LPS (1000
758 ng/ml) for 4 h, and co-localization of p65 and Vangl2 was detected by
759 immunofluorescence (p65, green; Vangl2, red; DAPI, blue).
760 **(H)** A structural diagram of Vangl2 as well as schematic representation of Myc-tagged
761 truncation mutants of Vangl2 (top). HEK293T cells were transfected with Flag-tagged
762 p65 and empty vector, Myc-tagged Vangl2 (FL) or Vangl2 truncation mutants. The cell
763 lysates were subjected to immunoprecipitation with anti-Flag beads and immunoblotted
764 with the indicated antibodies (bottom).
765 **(I)** HEK293T cells were transfected with Flag-tagged p65 and HA-tagged Vangl2 FL or
766 PkBD truncation. The cell lysates were subjected to immunoprecipitation with anti-Flag
767 beads and immunoblotted with the indicated antibodies.
768 **(J)** Luciferase activity in HEK293T cells transfected with an NF-κB luciferase reporter,
769 together with a vector encoding p65, along with the empty vector or with vectors
770 encoding Vangl2 or its truncation mutants. The results are presented relative to Renilla
771 luciferase activity.
772 IP, immunoprecipitation; WCL, whole-cell lysate. Data are representative of three
773 independent experiments and are plotted as the mean ±SD. *$p<0.05$, **$p<0.01$,
774 ***$p<0.001$ vs. corresponding control. NS, not significant.
775

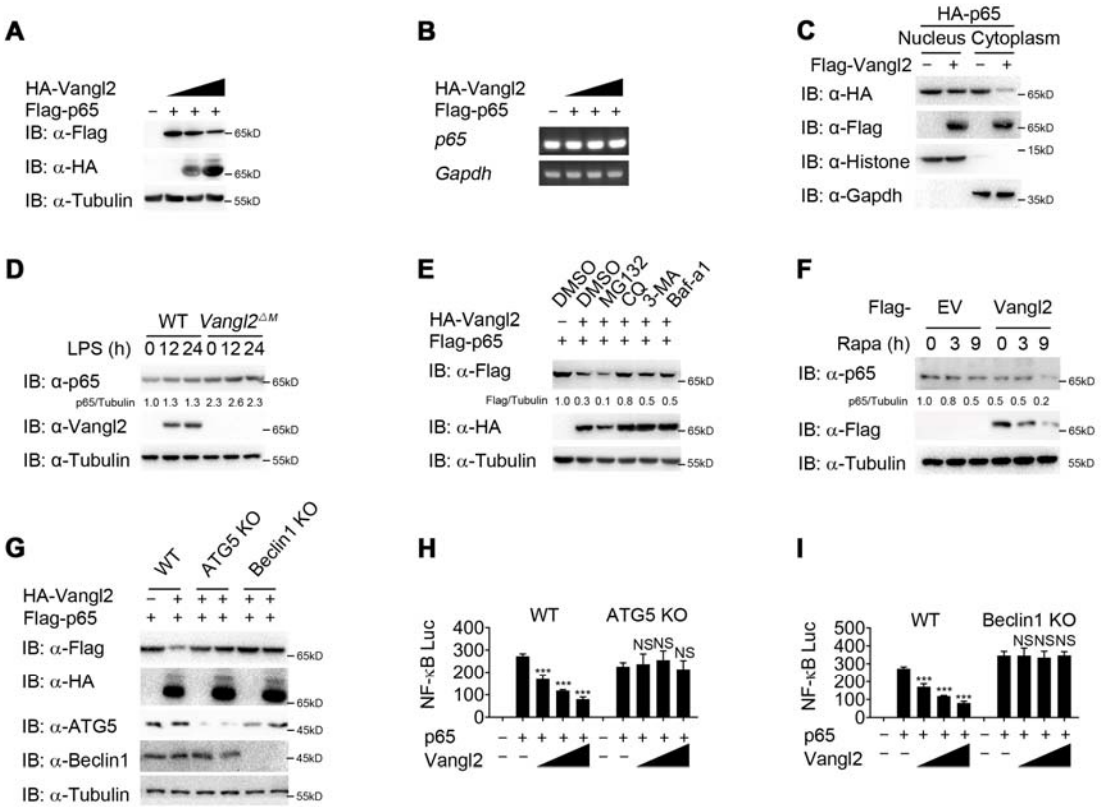

Figure 4. **Vangl2 promotes the autophagic degradation of p65.**

(A) Immunoblot analysis of HEK293T cells transfected with Flag-p65 and increasing amounts of the vector encoding HA-Vangl2 (0, 250, 500, and 1000 ng).

(B) Total RNA from HEK293T cells as in (A) was isolated and measured by semi-quantitative PCR.

(C) HEK293T cells transfected with Flag-p65 and increasing amounts of the vector encoding HA-Vangl2, and the expressions of p65 in nuclear or cytoplasm were detected by immunoblot.

(D) WT and Vangl2-deficient BMDMs were treated with LPS for the indicated times, and the expressions of p65 and Vangl2 were detected by immunoblot.

(E) HEK293T cells were transfected with Flag-p65 and HA-Vangl2 plasmids, and treated with DMSO, MG132 (10 μM), CQ (50 μM), 3-MA (10 mM) or Baf-A1 (0.2 μM) for 6 h. The cell lysates were analyzed by immunoblot.

791 **(F)** HEK293T cells were transfected with empty vector (EV) or Flag-Vangl2 plasmid, and
792 treated with rapamycin for the indicated times. The cell lysates were analyzed by
793 immunoblot with indicated antibodies.
794 **(G)** WT, ATG5 KO and Beclin1 KO HEK293T cells were transfected with Flag-p65,
795 together with or without HA-Vangl2 plasmids, and then the cell lysates were analyzed by
796 immunoblot with indicated antibodies.
797 **(H and I)** Luciferase activity in WT, ATG5 KO **(G)** and Beclin1 KO **(H)** HEK293T cells
798 transfected with plasmids encoding an NF-κB luciferase reporter and TK-Renilla reporter,
799 together with p65 plasmid along with increasing amounts of Vangl2, was measured at 24
800 h after transfection and normalized to the Renilla luciferase activity.
801 CHX, cycloheximide; 3-MA, 3-methyladenine; CQ, chloroquine; Baf A1, bafilomycin A1.
802 Data are representative of three independent experiments and are plotted as the mean
803 ±SD. *p<0.05, **p<0.01, ***p<0.001 vs. corresponding control. NS, not significant.
804
805
806
807
808
809
810
811

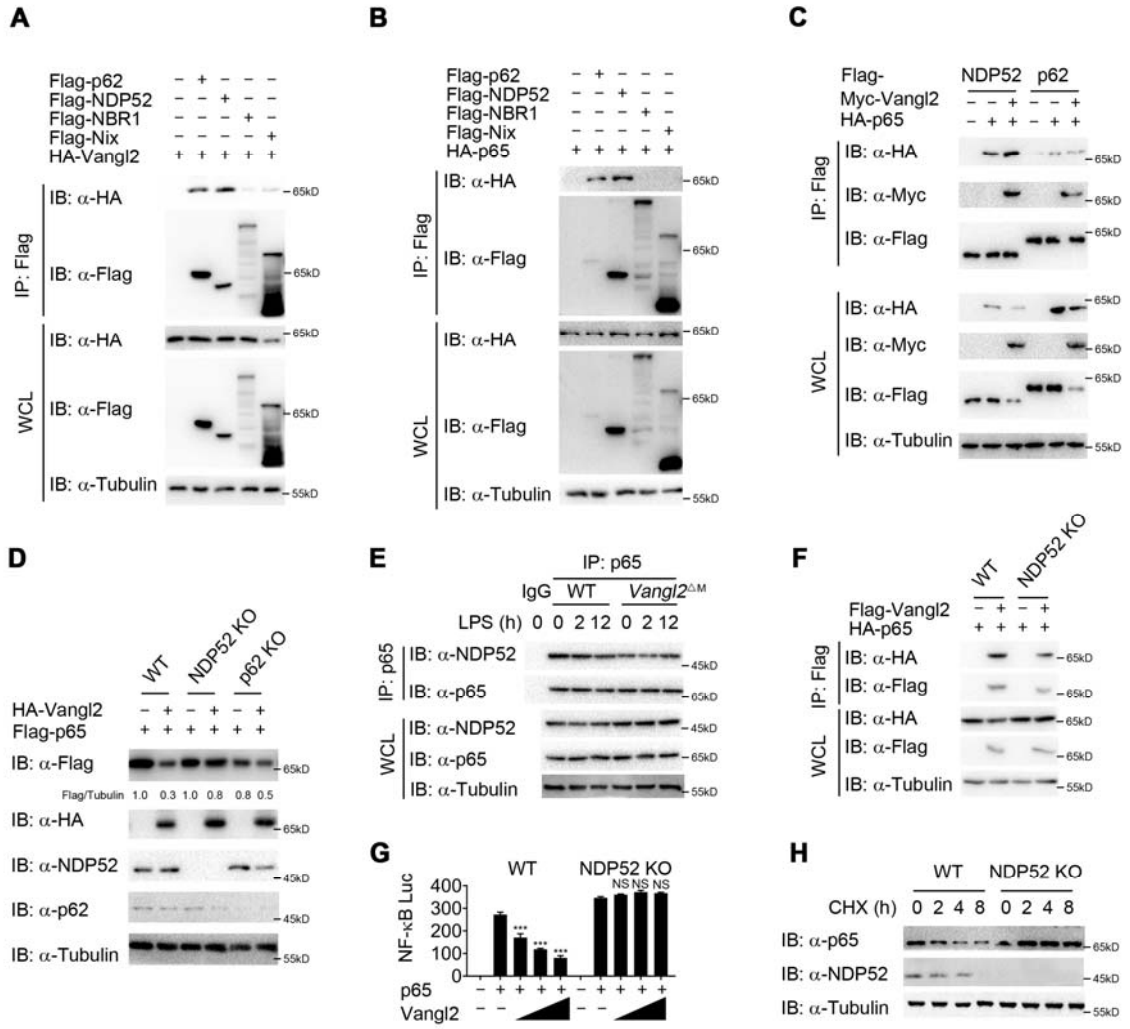

Figure 5. **Vangl2 enhances the recognition of p65 by cargo receptor NDP52.**

(A) HEK293T cells transfected with a vector expressing HA-Vangl2 along with the empty vector or vector encoding Flag-p62/NDP52/NBR1/Nix. The cell lysates were subjected to immunoprecipitation with anti-Flag beads and immunoblotted with the indicated antibodies.

(B) HEK293T cells transfected with a vector expressing HA-p65 along with the empty vector or vector encoding Flag-p62/NDP52/NBR1/Nix. The cell lysates were subjected to immuno-precipitation with anti-Flag beads and immunoblotted with the indicated antibodies.

(C) HEK293T cells were transfected with HA-p65 together with Flag-NDP52 or Flag-p62, as well as with empty vector or Myc-Vangl2. The cell lysates were subjected to

825 immunoprecipitation with anti-Flag beads and immunoblotted with the indicated
826 antibodies.
827 **(D)** WT, NDP52 KO and p62 KO HEK293T cells were transfected with a vector
828 expressing HA-p65 along with the empty vector or vector encoding Flag-Vangl2. The cell
829 lysates were immunoblotted with the indicated antibodies.
830 **(E)** WT and Vangl2-deficient BMDMs were stimulated with LPS (100 ng/ml) for the
831 indicated times. The cell lysates were subjected to immunoprecipitation with an anti-p65
832 antibody or control IgG and immunoblotted with the indicated antibodies.
833 **(F)** WT and NDP52 KO HEK293T cells were transfected with a vector expressing HA-
834 p65 along with the empty vector or vector encoding Flag-Vangl2. The cell lysates were
835 subjected to immunoprecipitation with anti-Flag beads and immunoblotted with the
836 indicated antibodies.
837 **(G)** Luciferase activity in WT and NDP52 KO HEK293T cells transfected with plasmids
838 encoding NF-κB luciferase reporter and TK-Renilla reporter, together with p65 plasmid
839 along with increasing amounts of Vangl2 plasmid, was measured at 24 h after
840 transfection.
841 **(H)** WT and NDP52 KO HEK293T were treated with CHX for the indicated times. The
842 cell lysates were immunoblotted with the indicated antibodies.
843 Data are representative of three independent experiments and are plotted as the mean
844 ±SD. *p<0.05, **p<0.01, ***p<0.001 vs. corresponding control. NS, not significant.

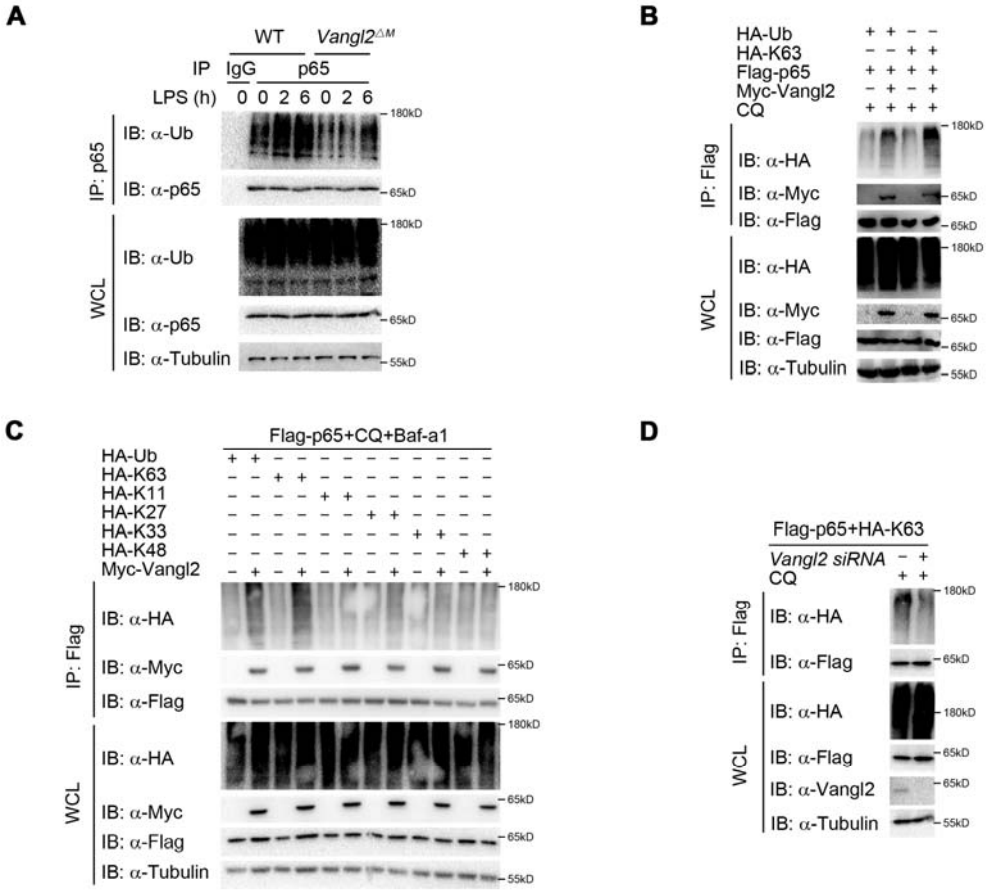

Figure 6. **Vangl2 increases the K63-linked ubiquitination of p65.**

(A) WT and Vangl2-deficient BMDMs were stimulated with LPS (100 ng/ml) for the indicated times. The cell lysates were subjected to immunoprecipitation with an anti-p65 antibody or control IgG and immunoblotted with the indicated antibodies.

(B) HEK293T cells were transfected with Flag-p65, Myc-Vangl2, HA-Ub or HA-K63 plasmids with the indicated combinations for 24 h and then treated with CQ for 8 h. The cell lysates were subjected to immunoprecipitation with anti-Flag beads and immunoblotted with the indicated antibodies.

(C) HEK293T cells were transfected with Flag-p65, Myc-Vangl2 and HA-Ub/K63/K11/K27/K33/K48 plasmids with the indicated combinations for 24 h and then treated with CQ and Baf-A1 for 8 h. The cell lysates were subjected to immunoprecipitation with anti-Flag beads and immunoblotted with the indicated antibodies.

860 **(D)** HEK293T cells were transfected with a vector expressing Flag-p65 and HA-K63
861 along with *Scramble* or *Vangl2* siRNA. The cell lysates were subjected to
862 immunoprecipitation with anti-Flag beads and immunoblotted with the indicated
863 antibodies.
864 Data are representative of three independent experiments.
865
866
867
868
869
870
871
872

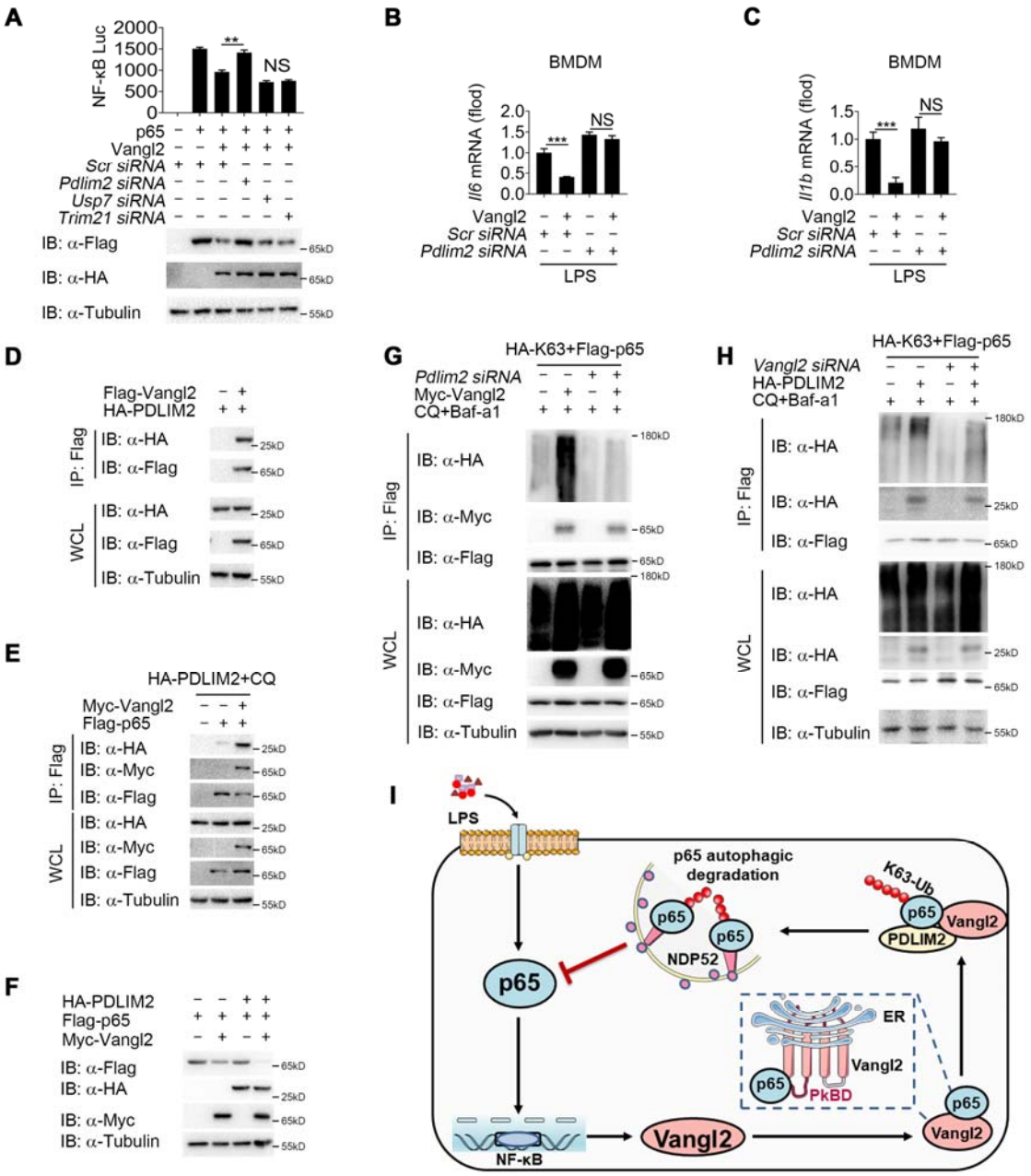

Figure 7. **Vangl2 recruits PDLIM2 to ubiquitinate p65.**

(A) HEK293T cells were transfected with the indicated siRNA, NF-κB reporter plasmids together with HA-Vangl2, Flag-p65 or the control vector as indicated for 24 h, and then subjected to luciferase assay and immunoblotting analysis.

(B and C) BMDMs were transfected with *Pdlim2* or *Scramble* siRNA along with the empty vector or vector encoding Flag-Vangl2, stimulated with LPS (100 ng/ml) for 6 h, then analyzed by qPCR for *Il6* **(B)** and *Il1b* **(C)** expression.

882 **(D)** HEK293T cells transfected with HA- PDLIM2 along with the empty vector or vector
883 encoding Flag-Vangl2. The cell lysates were subjected to immunoprecipitation with anti-
884 Flag beads and immunoblotted with the indicated antibodies.
885 **(E)** HEK293T cells were transfected with Flag-p65, HA-PDLIM2 and Myc-Vangl2
886 plasmids with the indicated combinations for 24 h and then treated with CQ and Baf-A1
887 for 8 h. The cell lysates were subjected to immunoprecipitation with anti-Flag beads and
888 immunoblotted with the indicated antibodies.
889 **(F)** HEK293T cells were transfected with Flag-p65, HA-PDLIM2 and Myc-Vangl2
890 plasmids with the indicated combinations for 24 h. The cell lysates were immunoblotted
891 with the indicated antibodies.
892 **(G)** HEK293T cells were transfected with Flag-p65, HA-K63 and Myc-Vangl2 plasmids,
893 the expression of E3 ubiquitin ligase was interfered with *Pdlim2* siRNA and then treated
894 with CQ and Baf-A1 for 8 h. The cell lysates were subjected to immunoprecipitation with
895 anti-Flag beads and immunoblotted with the indicated antibodies.
896 **(H)** HEK293T cells were transfected with *Pdlim2* or *Scramble* siRNA, along with or
897 without HA-PDLIM2, then treated with CQ and Baf-A1 for 8 h. The cell lysates were
898 subjected to immunoprecipitation with anti-Flag beads and immunoblotted with the
899 indicated antibodies.
900 **(I)** A schematic model to illustrate how Vangl2-PDLIM2-NDP52-p65 axis negatively
901 regulates NF-κB activation. During LPS stimulation, Vangl2 expression is up-regulated,
902 thus constituting a negative feedback loop to regulate NF-κB activation. In detail, Vangl2
903 functions as an adaptor protein to recruit an E3 ubiquitin ligase PDLIM2 to increase K63-
904 linked ubiquitination of p65 and promotes NDP52-mediated p65 degradation through
905 selective autophagy, resulting in ameliorating sepsis and suppressing production of pro-
906 inflammatory cytokines.
907 Data are representative of three independent experiments and are plotted as the mean
908 ±SD. *p<0.05, **p<0.01, ***p<0.001 vs. corresponding control. NS, not significant.
909

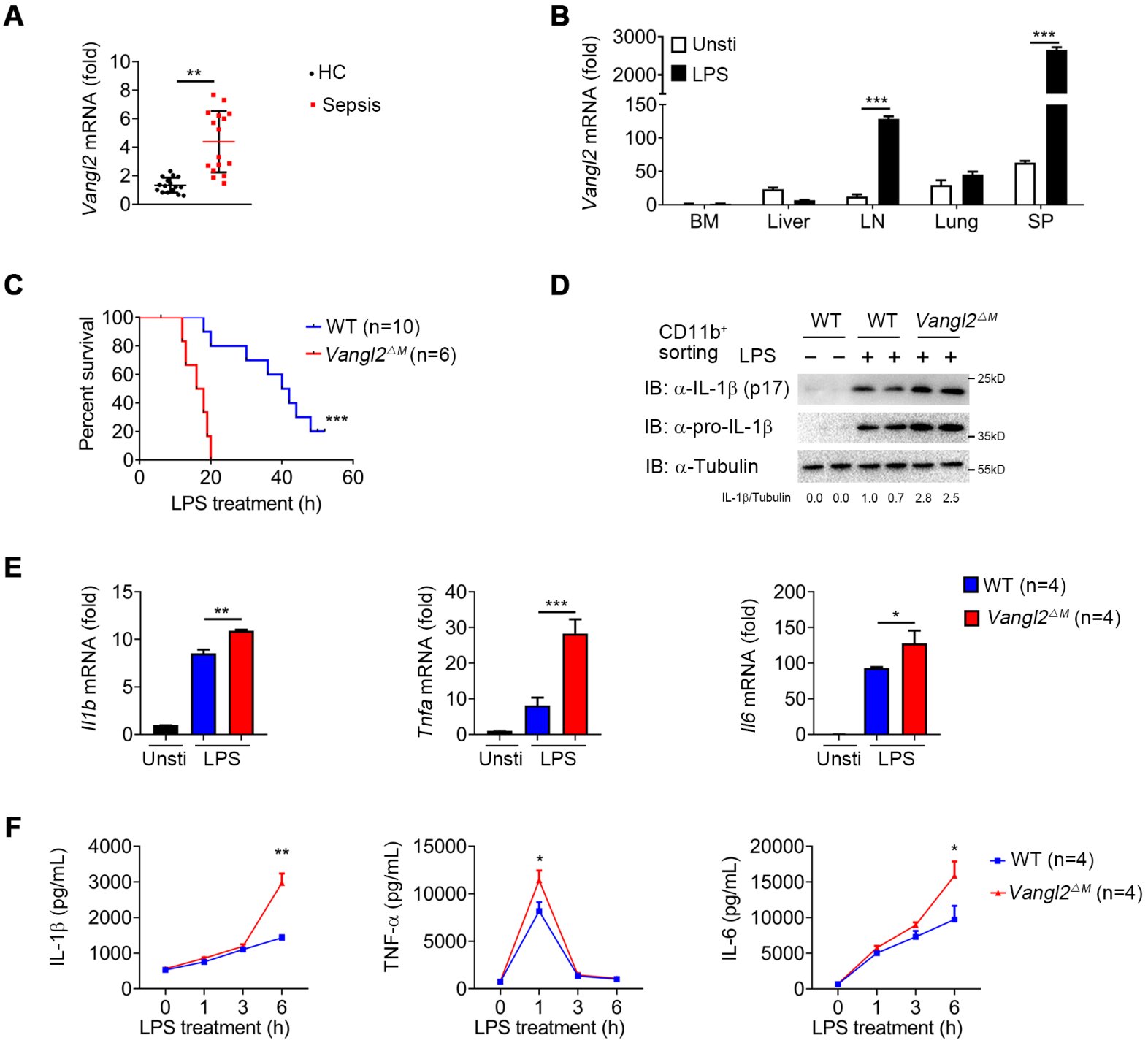
A
Vangl2 mRNA (fold)
10
8
6
4
2
0
**
HC
Sepsis
B
Vangl2 mRNA (fold)
3000
2000
150
100
50
0
Unsti
LPS
***
***
BM
Liver
LN
Lung
SP
C
Percent survival
100
80
60
40
20
0
WT (n=10)
Vangl2ΔM (n=6)
***
0
20
40
60
LPS treatment (h)
D
CD11b+ sorting
WT
WT
Vangl2ΔM
LPS
– – + + + +
IB: α-IL-1β (p17)
IB: α-pro-IL-1β
IB: α-Tubulin
25kD
35kD
55kD
IL-1β/Tubulin 0.0 0.0 1.0 0.7 2.8 2.5
E
Il1b mRNA (fold)
15
10
5
0
**
Unsti
LPS
Tnfa mRNA (fold)
40
30
20
10
0
***
Unsti
LPS
Il6 mRNA (fold)
200
150
100
50
0
*
Unsti
LPS
WT (n=4)
Vangl2ΔM (n=4)
F
IL-1β (pg/mL)
4000
3000
2000
1000
0
**
0
1
3
6
LPS treatment (h)
TNF-α (pg/mL)
15000
10000
5000
0
*
0
1
3
6
LPS treatment (h)
IL-6 (pg/mL)
20000
15000
10000
5000
0
*
0
1
3
6
LPS treatment (h)
WT (n=4)
Vangl2ΔM (n=4)

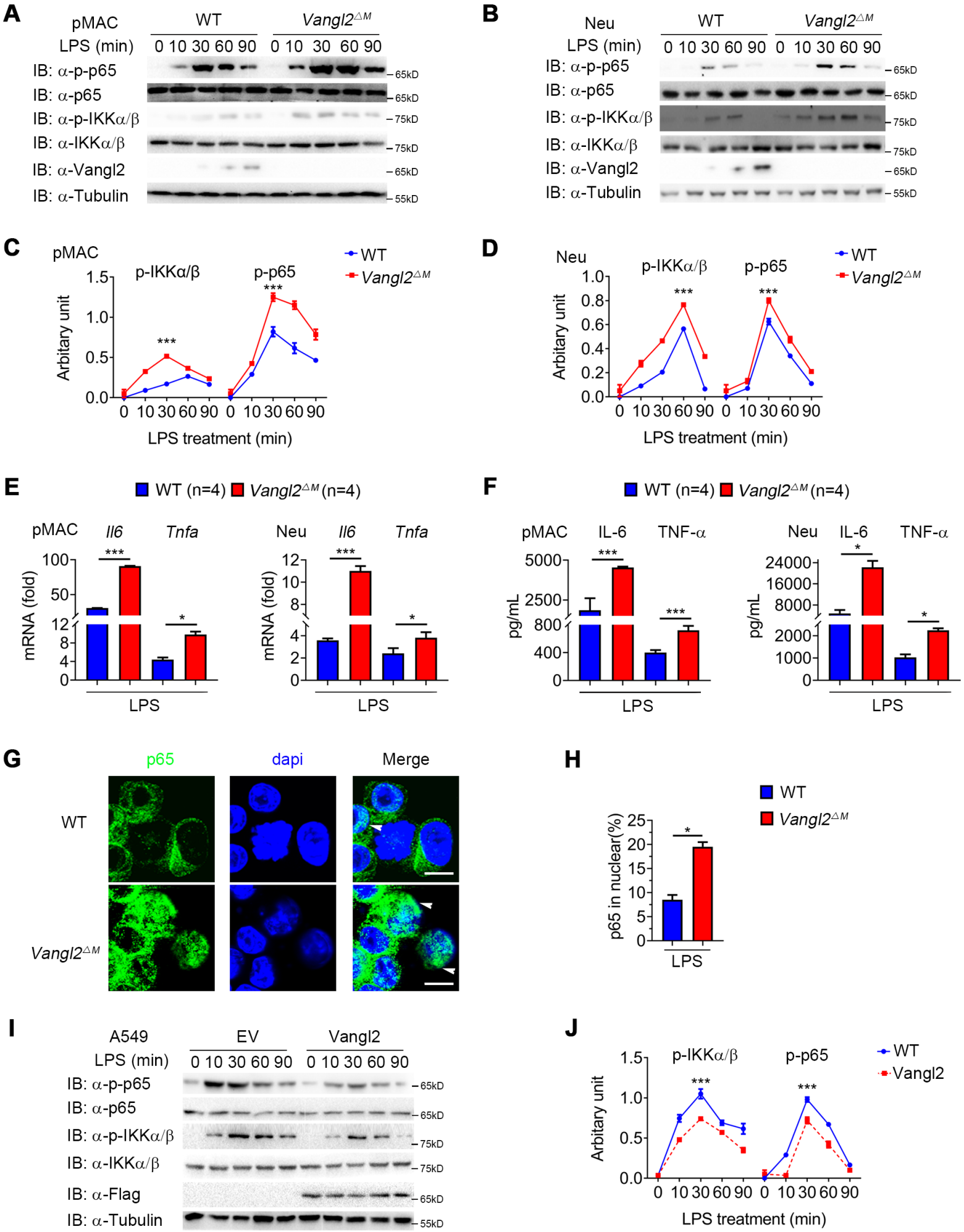
A
pMAC
WT
Vangl2ΔM
LPS (min)
0 10 30 60 90 0 10 30 60 90
IB: α-p-p65
IB: α-p65
IB: α-p-IKKα/β
IB: α-IKKα/β
IB: α-Vangl2
IB: α-Tubulin
65kD
75kD
55kD
B
Neu
WT
Vangl2ΔM
LPS (min)
0 10 30 60 90 0 10 30 60 90
IB: α-p-p65
IB: α-p65
IB: α-p-IKKα/β
IB: α-IKKα/β
IB: α-Vangl2
IB: α-Tubulin
C
pMAC
p-IKKα/β
p-65
WT
Vangl2ΔM
Arbitary unit
LPS treatment (min)
D
Neu
p-IKKα/β
p-p65
WT
Vangl2ΔM
Arbitary unit
LPS treatment (min)
E
WT (n=4) Vangl2ΔM (n=4)
pMAC
Il6
Tnfa
Neu
Il6
Tnfa
mRNA (fold)
LPS
F
WT (n=4) Vangl2ΔM (n=4)
pMAC
IL-6
TNF-α
Neu
IL-6
TNF-α
pg/mL
LPS
G
p65
dapi
Merge
WT
Vangl2ΔM
H
WT
Vangl2ΔM
p65 in nuclear(%)
LPS
I
A549
EV
Vangl2
LPS (min)
0 10 30 60 90 0 10 30 60 90
IB: α-p-p65
IB: α-p65
IB: α-p-IKKα/β
IB: α-IKKα/β
IB: α-Flag
IB: α-Tubulin
J
p-IKKα/β
p-p65
WT
Vangl2
Arbitary unit
LPS treatment (min)

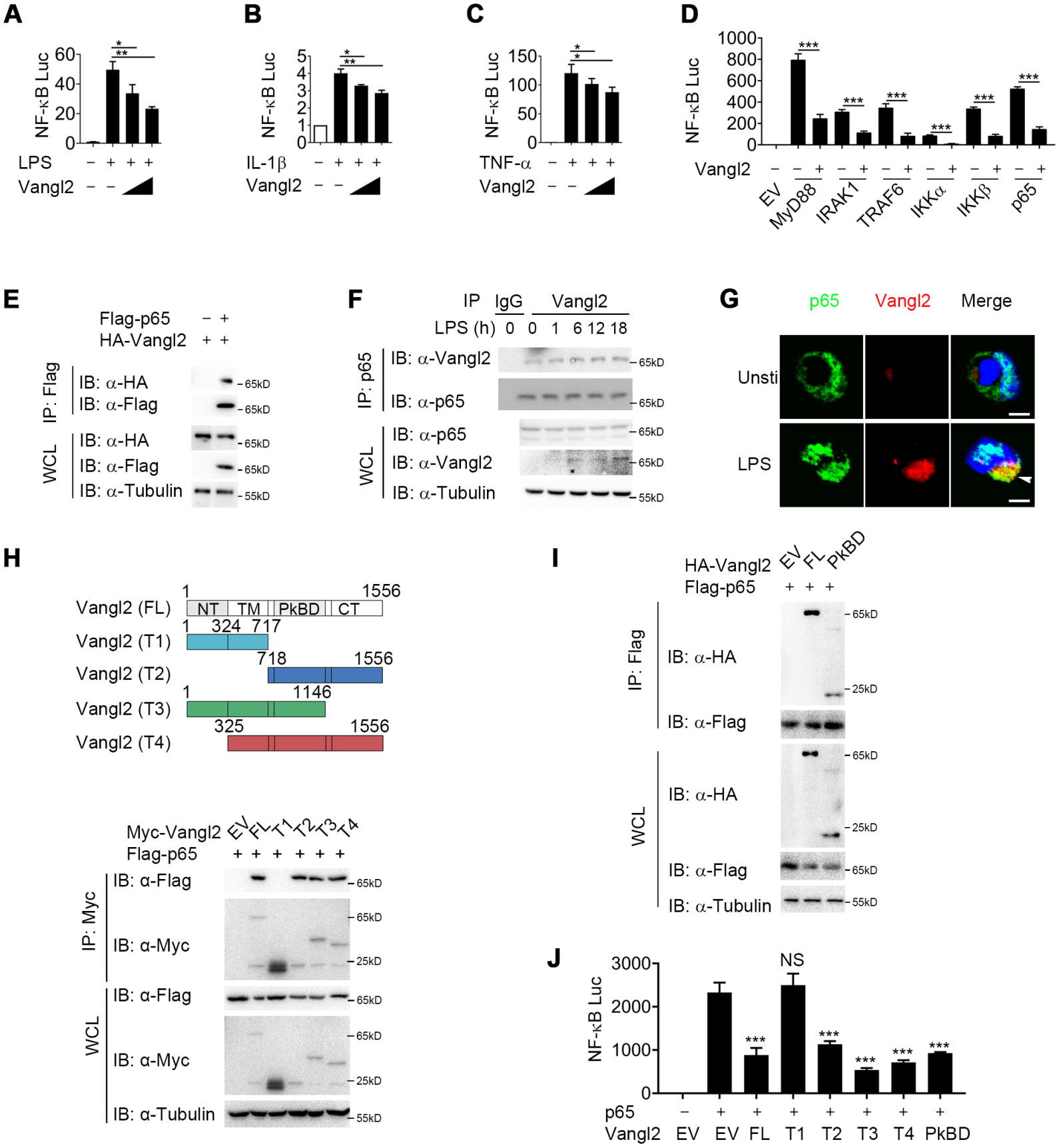
A
NF-κB Luc
LPS
Vangl2
B
IL-1β
C
TNF-α
D
EV
MyD88
IRAK1
TRAF6
IKKα
IKKβ
p65
E
Flag-p65
HA-Vangl2
IP: Flag
IB: α-HA
IB: α-Flag
WCL
IB: α-Tubulin
65kD
55kD
F
IP
IgG
Vangl2
LPS (h)
IP: p65
IB: α-Vangl2
IB: α-p65
G
p65
Vangl2
Merge
Unsti
LPS
H
Vangl2 (FL)
NT
TM
PkBD
CT
Vangl2 (T1)
Vangl2 (T2)
Vangl2 (T3)
Vangl2 (T4)
Myc-Vangl2
IP: Myc
IB: α-Myc
I
HA-Vangl2
Flag-p65
25kD
J
NS
p65
Vangl2

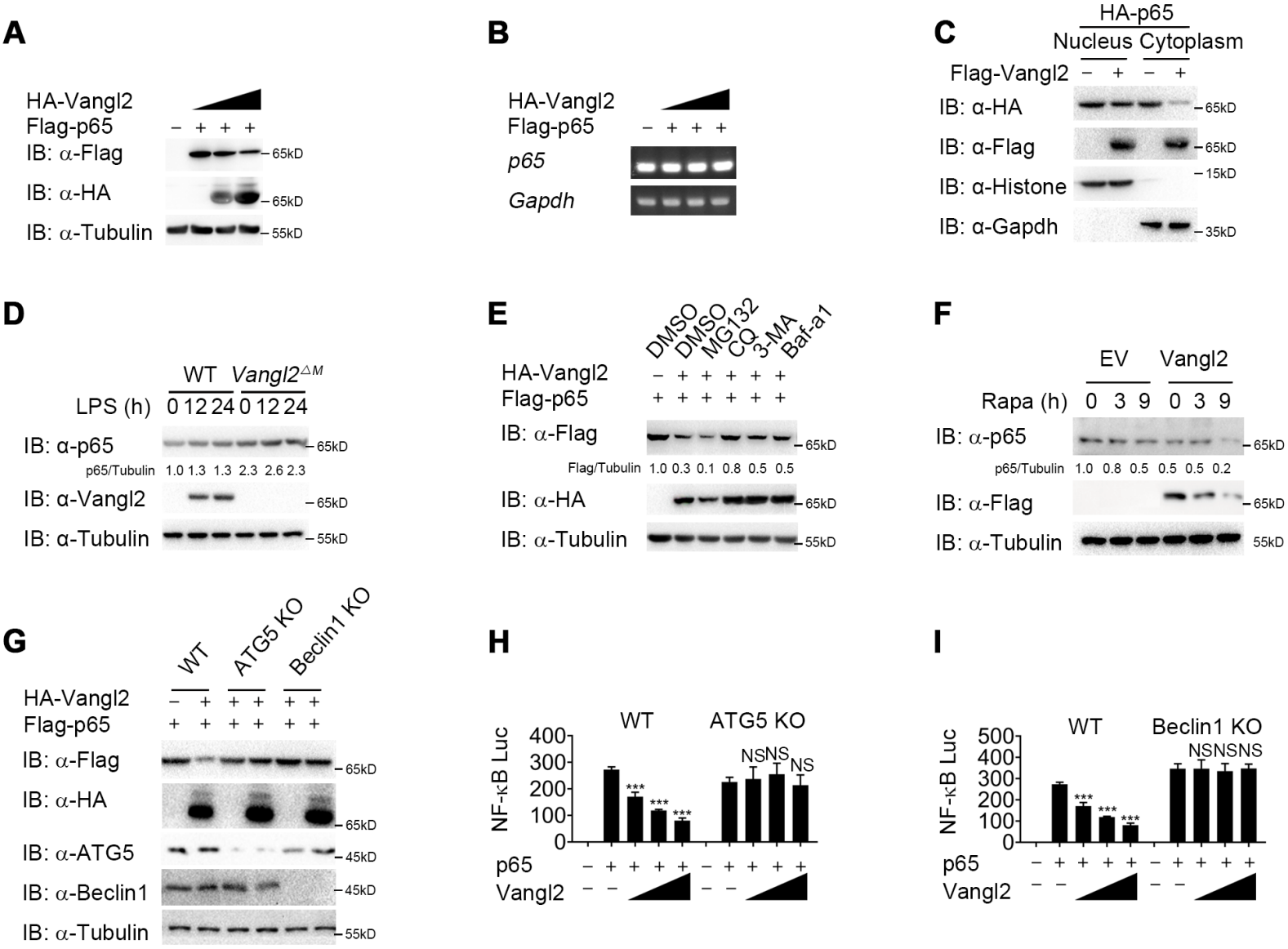
A
HA-Vangl2
Flag-p65
– + + +
IB: α-Flag
IB: α-HA
IB: α-Tubulin
65kD
65kD
55kD
B
HA-Vangl2
Flag-p65
– + + +
p65
Gapdh
C
HA-p65
Nucleus Cytoplasm
Flag-Vangl2 – + – +
IB: α-HA
IB: α-Flag
IB: α-Histone
IB: α-Gapdh
65kD
65kD
15kD
35kD
D
WT Vangl2ΔM
LPS (h) 0 12 24 0 12 24
IB: α-p65
p65/Tubulin 1.0 1.3 1.3 2.3 2.6 2.3
IB: α-Vangl2
IB: α-Tubulin
65kD
65kD
55kD
E
DMSO DMSO MG132 CQ 3-MA Baf-a1
HA-Vangl2 – + + + + +
Flag-p65 + + + + + +
IB: α-Flag
Flag/Tubulin 1.0 0.3 0.1 0.8 0.5 0.5
IB: α-HA
IB: α-Tubulin
65kD
65kD
55kD
F
EV Vangl2
Rapa (h) 0 3 9 0 3 9
IB: α-p65
p65/Tubulin 1.0 0.8 0.5 0.5 0.5 0.2
IB: α-Flag
IB: α-Tubulin
65kD
65kD
55kD
G
WT ATG5 KO Beclin1 KO
HA-Vangl2 – + + + + +
Flag-p65 + + + + + +
IB: α-Flag
IB: α-HA
IB: α-ATG5
IB: α-Beclin1
IB: α-Tubulin
65kD
65kD
45kD
45kD
55kD
H
WT ATG5 KO
NF-κB Luc
400
300
200
100
0
***
NS
p65 – + + + + – + + + +
Vangl2 – – – –
I
WT Beclin1 KO
NF-κB Luc
500
400
300
200
100
0
***
NS
p65 – + + + + – + + + +
Vangl2 – – – –

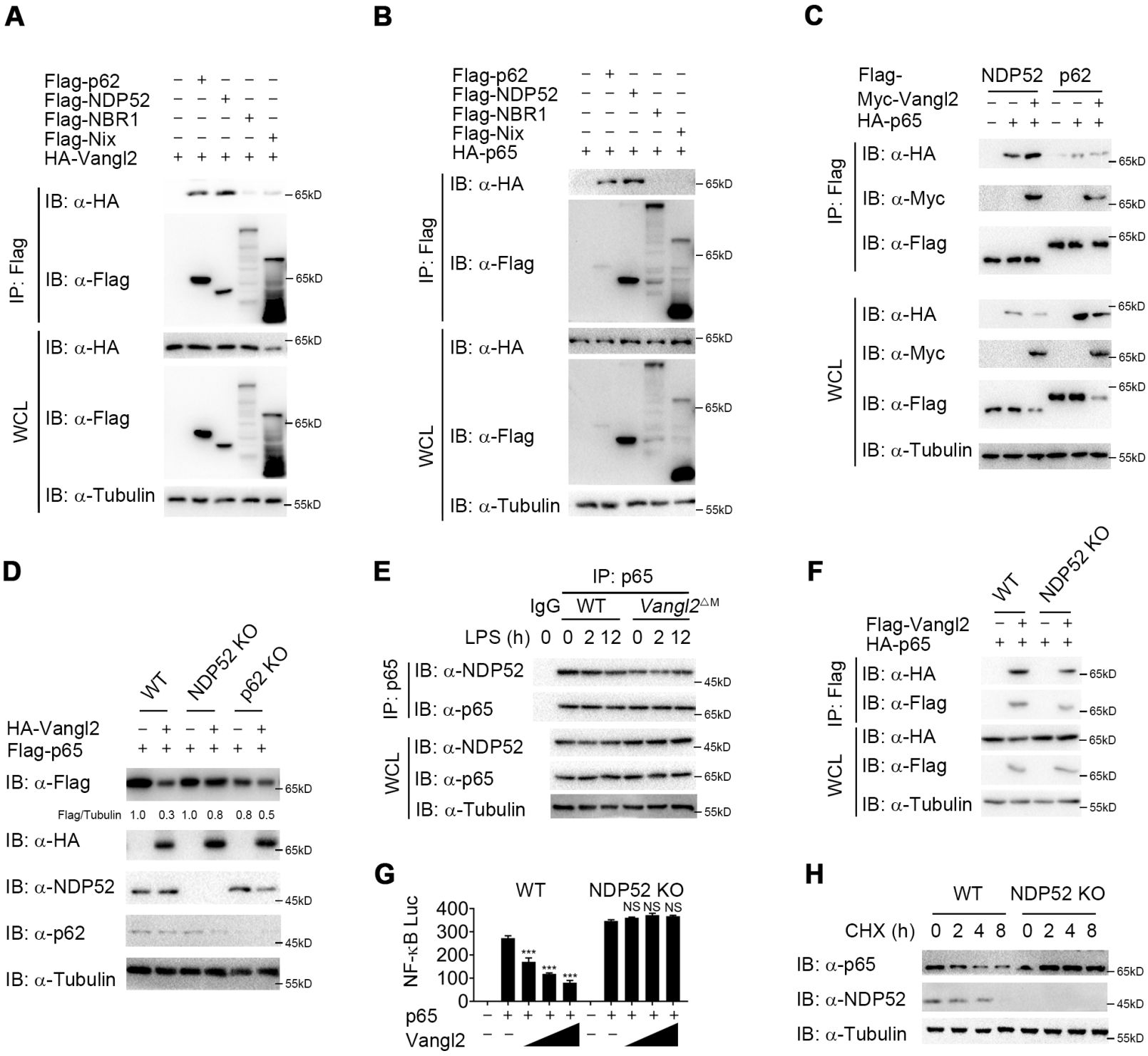
A
Flag-p62
Flag-NDP52
Flag-NBR1
Flag-Nix
HA-Vangl2
IP: Flag
IB: α-HA
IB: α-Flag
WCL
IB: α-HA
IB: α-Flag
IB: α-Tubulin
65kD
55kD
B
Flag-p62
Flag-NDP52
Flag-NBR1
Flag-Nix
HA-p65
IP: Flag
IB: α-HA
IB: α-Flag
WCL
IB: α-HA
IB: α-Flag
IB: α-Tubulin
65kD
55kD
C
Flag-
Myc-Vangl2
HA-p65
NDP52
p62
IP: Flag
IB: α-HA
IB: α-Myc
IB: α-Flag
WCL
IB: α-HA
IB: α-Myc
IB: α-Flag
IB: α-Tubulin
65kD
55kD
D
WT
NDP52 KO
p62 KO
HA-Vangl2
Flag-p65
IB: α-Flag
Flag/Tubulin 1.0 0.3 1.0 0.8 0.8 0.5
IB: α-HA
IB: α-NDP52
IB: α-p62
IB: α-Tubulin
65kD
45kD
55kD
E
IP: p65
IgG
WT
Vangl2ΔM
LPS (h) 0 0 2 12 0 2 12
IP: p65
IB: α-NDP52
IB: α-p65
WCL
IB: α-NDP52
IB: α-p65
IB: α-Tubulin
45kD
65kD
55kD
F
WT
NDP52 KO
Flag-Vangl2
HA-p65
IP: Flag
IB: α-HA
IB: α-Flag
WCL
IB: α-HA
IB: α-Flag
IB: α-Tubulin
65kD
55kD
G
WT
NDP52 KO
NF-κB Luc
400
300
200
100
0
***
NS
p65
Vangl2
H
WT
NDP52 KO
CHX (h) 0 2 4 8 0 2 4 8
IB: α-p65
IB: α-NDP52
IB: α-Tubulin
65kD
45kD
55kD

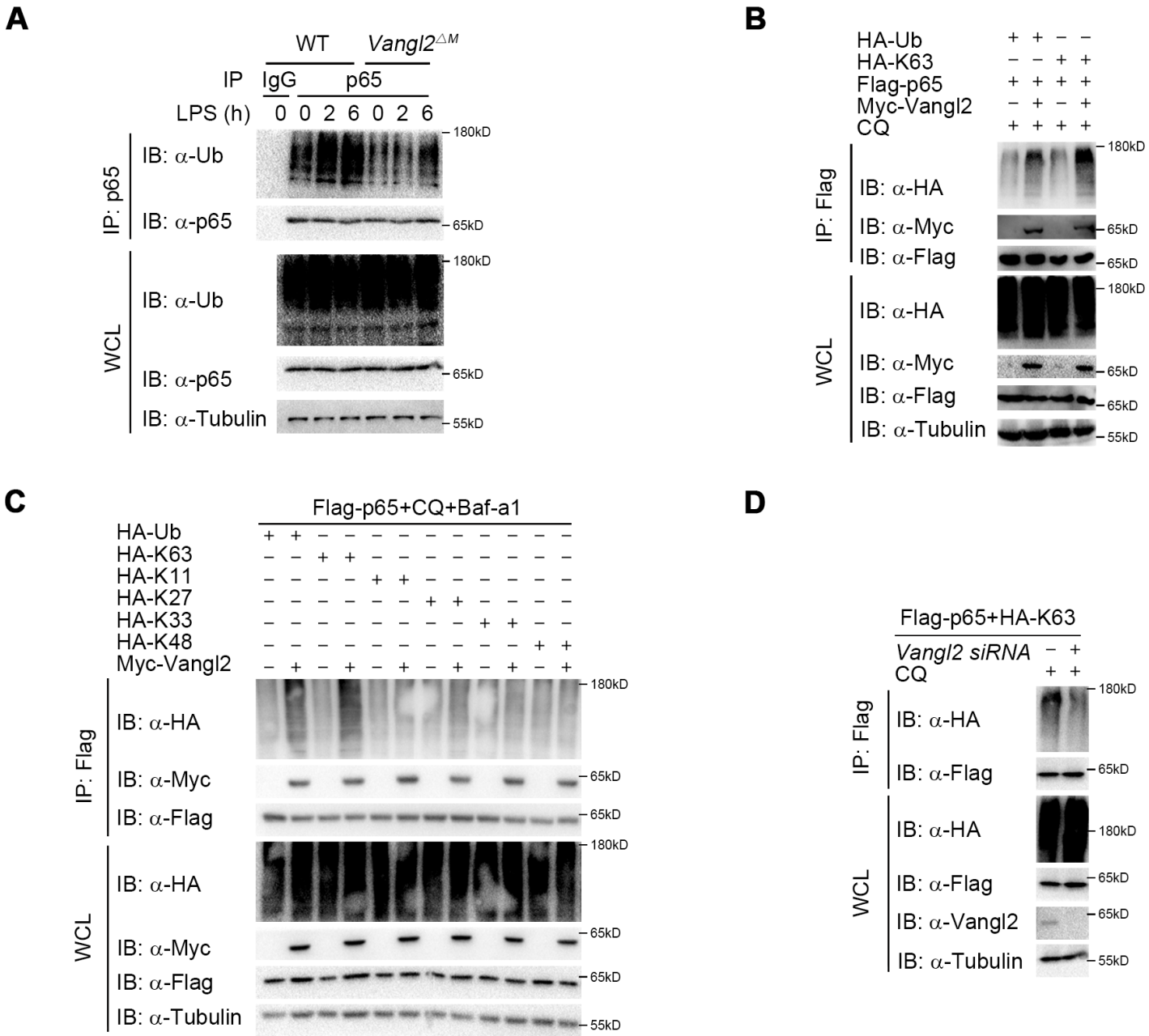
A
WT
Vangl2△M
IP
IgG
p65
LPS (h)
0 0 2 6 0 2 6
IP: p65
IB: α-Ub
IB: α-p65
WCL
IB: α-Ub
IB: α-p65
IB: α-Tubulin
180kD
65kD
55kD
B
HA-Ub
HA-K63
Flag-p65
Myc-Vangl2
CQ
IP: Flag
IB: α-HA
IB: α-Myc
IB: α-Flag
WCL
IB: α-HA
IB: α-Myc
IB: α-Flag
IB: α-Tubulin
180kD
65kD
55kD
C
Flag-p65+CQ+Baf-a1
HA-Ub
HA-K63
HA-K11
HA-K27
HA-K33
HA-K48
Myc-Vangl2
IP: Flag
IB: α-HA
IB: α-Myc
IB: α-Flag
WCL
IB: α-HA
IB: α-Myc
IB: α-Flag
IB: α-Tubulin
180kD
65kD
55kD
D
Flag-p65+HA-K63
Vangl2 siRNA
CQ
IP: Flag
IB: α-HA
IB: α-Flag
WCL
IB: α-HA
IB: α-Flag
IB: α-Vangl2
IB: α-Tubulin
180kD
65kD
55kD

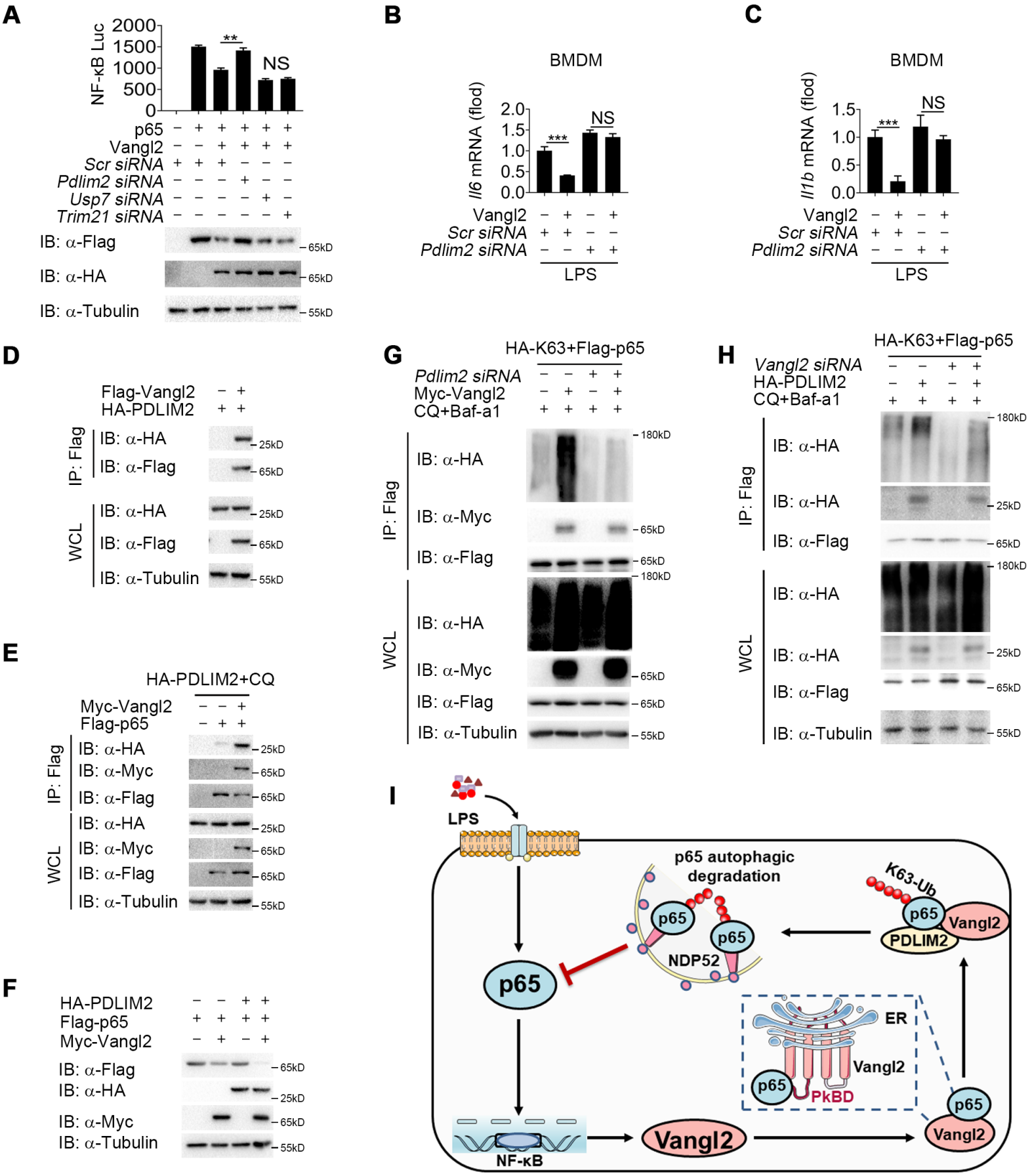
A
NF-κB Luc
2000
1500
1000
500
0
**
NS
p65
Vangl2
Scr siRNA
Pdlim2 siRNA
Usp7 siRNA
Trim21 siRNA
IB: α-Flag
IB: α-HA
IB: α-Tubulin
65kD
55kD
B
BMDM
Il6 mRNA (flod)
2.0
1.5
1.0
0.5
0.0
***
NS
Vangl2
Scr siRNA
Pdlim2 siRNA
LPS
C
BMDM
Il1b mRNA (flod)
1.5
1.0
0.5
0.0
***
NS
Vangl2
Scr siRNA
Pdlim2 siRNA
LPS
D
Flag-Vangl2
HA-PDLIM2
IP: Flag
WCL
IB: α-HA
IB: α-Flag
IB: α-Tubulin
25kD
65kD
55kD
E
HA-PDLIM2+CQ
Myc-Vangl2
Flag-p65
IP: Flag
WCL
IB: α-HA
IB: α-Myc
IB: α-Flag
IB: α-Tubulin
25kD
65kD
55kD
F
HA-PDLIM2
Flag-p65
Myc-Vangl2
IB: α-Flag
IB: α-HA
IB: α-Myc
IB: α-Tubulin
65kD
25kD
55kD
G
HA-K63+Flag-p65
Pdlim2 siRNA
Myc-Vangl2
CQ+Baf-a1
IP: Flag
WCL
IB: α-HA
IB: α-Myc
IB: α-Flag
IB: α-Tubulin
180kD
65kD
55kD
H
HA-K63+Flag-p65
Vangl2 siRNA
HA-PDLIM2
CQ+Baf-a1
IP: Flag
WCL
IB: α-HA
IB: α-Flag
IB: α-Tubulin
180kD
25kD
65kD
55kD
I
LPS
p65 autophagic degradation
K63-Ub
p65
Vangl2
PDLIM2
NDP52
ER
PkBD
NF-κB